IN-47
045805

Atmospheric Torques on the Solid Earth and Oceans based on the GEOS-1 General Circulation Model

Braulio V. Sánchez

Space Geodesy Branch
Laboratory for Terrestrial Physics
NASA Goddard Space Flight Center
Greenbelt, Maryland 20771

Andrew Y. Au

Raytheon ITSS Corporation
Lanham, Maryland

Abstract

The **GEOS-1** general circulation model has been used to compute atmospheric torques on the oceans and solid Earth for the period 1980-1995. The time series for the various torque components have been analyzed by means of Fourier transform techniques.

It was determined that the wind stress torque over land is more powerful than the wind stress torque over water by 55%, 42%, and 80% for the x, y, and z components respectively. This is mainly the result of power in the high frequency range.

The pressure torques due to polar flattening, equatorial ellipticity, marine geoid, and continental orography were computed. The orographic or "mountain torque" components are more powerful than their wind stress counterparts (land plus ocean) by 231% (x), 191% (y), and 77% (z). The marine pressure torques due to geoidal undulations are much smaller than the orographic ones, as expected. They are only 3% (x), 4% (y), and 5% (z) of the corresponding mountain torques. The geoidal pressure torques are approximately equal in magnitude to those produced by the equatorial ellipticity of the Earth. The pressure torque due to polar flattening makes the largest contributions to the atmospheric torque budget. It has no zonal component, only equatorial ones. Most of the power of the latter, between 68% and 69%, is found in modes with periods under 15 days. The single most powerful mode has a period of 361 days.

The gravitational torque ranks second in power only to the polar flattening pressure torque. Unlike the former, it does produce a zonal component, albeit much smaller (1%) than the equatorial ones. The gravitational and pressure torques have opposite signs, therefore, the gravitational torque nullifies 42% of the total pressure torque. Zonally, however, the gravitational torque amounts to only 6% of the total pressure torque.

The power budget for the total atmospheric torque yields 7595 and 7120 Hadleys for the equatorial components and 966 Hadleys for the zonal. The x-component exhibits a large mean value (1811 H), mainly the result of polar flattening pressure torque acting on the ocean surfaces. Atmospheric torque modes with periods of 408, 440, and 476 days appear in the spectrum of the equatorial components.

1. Introduction.

Atmospheric torques on the body of the Earth are produced by forces arising from three distinct physical processes : tangential stresses (surface friction), normal stresses (pressure), and body forces (gravitation).

The wind stress torques are produced by the momentum transfer due to the motion of the air over land and ocean surfaces. The normal stresses require two conditions to produce a torque : topographic features and a pressure distribution producing a non-vanishing (and non-radial) resultant. The main topographic feature on the Earth is its ellipticity of figure, or flattening. Higher degree components are embodied by local features such as mountain ranges on the continents, and by the geoidal undulations over the oceans. The gravitational torques arise from the non-radial part of the Earth's gravitational field.

The nature of the transmission of oceanic atmospheric torques to the solid Earth is represented by a transfer function, i.e., an ocean model. Possible modes include the following :

- Inverted Barometer : there is no transmission of water surface forces to the mantle.
- Dynamic Response : transmission occurs through the dynamics of an ocean model.
- Non-inverted Barometer : transmission occurs instantaneously.

Analysis by Wahr (1982) indicate that for forcing periods longer than 10 days the ocean should respond in the inverted barometer mode. More recently, Ponte (1993) concluded that sea level response is strongly dependent on frequency and location, with the largest departures from inverted barometer behavior occurring at short periods and near boundaries. However, he reports significant nonisostatic variability at periods as long as 11-15 days, due to dynamic excitation of large scale normal modes.

Dehant et al. (1996) evaluated effects of the S1 solar barometric tide, they considered both extreme cases of inverted barometer and non-inverted barometer responses, as well as various topographic features (ellipsoid, geoid, continental topography, ocean floor bathymetry).

Segschneider and Sundermann (1997) observe two effects which contribute to the ocean pressure torque :

- Sea level : higher at the western boundaries, due to the steady westward blowing trade winds.
- Density : depth of the thermocline decreases from west to east.

They determine that sea level and density stratification are almost in isostatic balance within a time step of 1 month. The net torque is 2 orders of magnitude smaller than the effect of sea level alone, with sea level effects slightly dominant. Furthermore, they determine that wind friction torque input to the ocean is equal to net pressure torque from the ocean to the solid Earth. However, if the time step is less than the speed of barotropic modes, the response could be dynamic.

In order to compute the wind stress torque over the oceans, it is customary to express the relationship between the stress, Γ, and the velocity, $\mathbf{U}(10)$, measured at a single height (10 meters) above the mean surface by the expression :

$$\Gamma = C_{DN}(10)\ \rho\ |\ \mathbf{U}(10)\ |\ \mathbf{U}(10)$$

C_{DN} is the neutral drag coefficient, ρ is the air density.

Let $U(10) = |\ \mathbf{U}(10)\ |$

$C_{DN}(10)$ as a function of U(10) over the sea has been given in the literature by a number of investigators, including Wu (1969, 1980), Garratt (1977), Large and Pond (1981), Amorocho and DeVries (1980).

The neutral drag coefficient corresponds to the height at which the magnitudes of mechanical and thermal production of turbulence are equal, also referred to as the Monin-Obukhov length (L). It is the height above the ground where buoyant forces become comparable to the mechanical or sheer related forces in generating turbulence. At a given height "z" conditions can be unstable, neutral, or stable :

unstable: $(z/L) < 0$

neutral: $(z/L) = 0$

stable: $(z/L) > 0$

The Monin-Obukhov length is a function of a number of variables, including thermodynamic parameters such as the sensible heat flux at the surface, the absolute temperature and the specific heat at constant pressure.

The modification of the neutral drag coefficient to account for non-neutral conditions is done by means of Similarity functions of the ratio (z/L), the specific functional form depends on the value of this ratio. Bunker (1976) provides a table of modified drag coefficient values as a function of wind speed and "air minus sea temperature class".

Swinbank (1985) computed orographic and stress torques for a period of 4 months during 1978-1979, using the United Kingdom Meteorological Office general circulation model. His results indicate mountain torque as the main contributor to short-term variability in global atmospheric angular momentum.

Boer (1990) used data from a 20-year climate simulation using the Canadian Climate Centre general circulation model with 5.625° space resolution and 18 hour time sampling. He found that on time scales of days the orographic and stress torques contribute to the rate of change of angular momentum in the ratio 60-40%. In time scales of days to months the sum of orographic pressure torque and land stress contribute 85-90% to the variation of angular momentum.

Rosen (1993) offers an informative discussion of the literature on the torque problem.

Bryan (1997) made use of wind stress fields from the ECMWF and the Hellerman-Rosenstein global atmospheric models, the globally integrated wind stress ocean torques for the two models show a difference in sign.

The determination of the wind stress over land is more complicated. Some of the early formulations are in terms of the geostrophic velocity and a geostrophic drag coefficient, i.e., Cressman (1960), LaValle and Girolamo (1975), and Garratt (1977). More recently, Wahr and Oort (1984) assumed that the greater viscous coupling over land acts to decrease the surface wind speeds in such a way that the zonal stress over land and ocean remains the same. They recognize this assumption to be invalid in latitudes between 0° and 30° North where the local surface winds associated with the monsoon are eastward, concentrated mainly over land, while the zonally averaged winds over the ocean are westward.

The purpose of this investigation is to compute and analyze the various atmospheric torques associated with the global stress and pressure fields provided by the Goddard Earth Observing System (**GEOS**) General Circulation Model.

2. The Goddard Earth Observing System General Circulation Model, Version 1, (GEOS-1).

The GEOS-1 model was produced by the Data Assimilation Office at NASA's Goddard Space Flight Center. It has a global resolution of 2° latitude by 2.5° longitude, with data points every 3 hours, it covers the period 1980-1995.

The stress fields incorporate space and time dependent variations for water, sea ice, permanent ice, and land surfaces. Monthly varying climatological roughness lengths are specified for each land surface vegetation type.

Surface stress calculations incorporate the Monin-Obukhov stability theory and corresponding similarity functions. Surface geopotential heights are obtained by averaging of the Navy 10' by 10' dataset supplied by the National Center for Atmospheric Research (NCAR).

The model incorporates data from a variety of sources :

- Conventional Sources : rawinsondes, dropwindsondes, rocketsondes, ships, buoys, surface stations, and aircraft.
- Satellite Sources : cloud track winds derived from geostationary imagery, i.e., the GOES satellite. Thickness retrievals from the TIROS operational vertical sounder flying on operational polar-orbiting satellites.
- Lower boundary conditions :

(i) Sea surface temperature from values provided by the Climate Prediction Center at the National Centers for Environmental Prediction (NCEP) and the Center for Ocean, Land and Atmosphere (COLA). These consist of blended satellite and in situ observations.
(ii) Soil moisture from observed monthly mean surface air temperature and precipitation.

More detailed information is given by Schubert et al. (1997), and by Takacs et al. (1994).

3. Wind Stress Torques.

The torques produced by the various forces are computed by forming the appropriate vector products. The resulting equations for the wind stress torques are given below.

Let,

i, j, k : unit vectors in the (x, y, z) geographic coordinate system.

r : radius vector.

$r = | \mathbf{r} |$

θ : colatitude.
λ : longitude.

$\mathbf{u}_r$, $\mathbf{u}_\theta$, $\mathbf{u}_\lambda$: unit vectors in the (r, θ, λ) geographic coordinate system.

Γ : wind stress vector.

$$\Gamma = \Gamma_r \mathbf{u}_r + \Gamma_\theta \mathbf{u}_\theta + \Gamma_\lambda \mathbf{u}_\lambda$$

per unit area :

$$\mathbf{r} \times \Gamma = (- \Gamma_\theta \, r \sin\lambda - \Gamma_\lambda \, r \cos\theta \cos\lambda) \, \mathbf{i}$$

$$+ (\Gamma_\theta \, r \cos\lambda - \Gamma_\lambda \, r \cos\theta \sin\lambda) \, \mathbf{j}$$

$$+ \Gamma_\lambda \, r \sin\theta \, \mathbf{k}$$

The geographic global distribution of wind stress torque at a specific time is displayed in Fig. 3.1. The time series corresponding to the wind stress torque have been analyzed by means of Fourier Transform methods. The percentages of total power for periods under 15 days for the (x, y, z) components are (74%, 72%, 72.7%) for the ocean, and (85.7%, 86.5%, 87.9%) for land. The land torque subdaily variability exceeds that of the ocean torque in ratios of 3.47, 3.42, and 4.25 for x, y, and z-components, many daily and half-daily modes appear prominently in the land torque spectrum. The ocean torque equatorial components exhibit larger seasonal variability than the land counterparts. The annual variability is most pronounced in the ocean zonal component, due to one single mode with period of 361.2 days. The ocean torque has more power than the land torque for all three components in the interannual range.

4. Pressure Torques.

The equations used for the computation of the pressure torque are the following,

Let,

p_s : atmospheric pressure.

n : unit vector, local outward normal to topographic surface.

H : topography.

per unit area :

$$\mathbf{r} \times (-p_s \mathbf{n}) = -p_s \{ [(\partial H/\partial\lambda) \cot\theta \cos\lambda + (\partial H/\partial\theta) \sin\lambda] \mathbf{i}$$

$$+ [(\partial H/\partial\lambda) \cot\theta \sin\lambda - (\partial H/\partial\theta) \cos\lambda)] \mathbf{j}$$

$$- (\partial H/\partial\lambda) \mathbf{k} \}$$

In the developments that follow, the pressure torque is analyzed according to the particular topographic features represented by "H". The continental topography over land and the geoidal undulations over the ocean are treated separately, as well as the polar flattening and the equatorial ellipticity of the Earth.

The partial derivatives of the marine geoidal undulations and the continental topography have been computed by means of central-difference approximations. Formulations involving three, five, seven, and nine points were tested. No significant variations were found in the results. The three point method was adopted for the long range computations.

4.1. Marine Geoid Pressure Torque.

The geoidal undulations used to compute the pressure torque over the oceans are those associated with the EGM96 gravity field model. They are accurate to better than one meter in most areas. More details about the EGM96 gravity field are given in section 5.

The geographic global distribution of marine geoid pressure torque at a specific time is displayed in Fig. 4.1.1. Fourier spectral analysis indicates zonal component power in the subdaily range is greater than the equatorial, the three top contributing modes have daily and half-daily periods. The equatorial components show greater annual variability, produced by a single mode with period of 357.5 days.

4.2. Orographic Torque.

The calculation of the pressure torque over the continents requires the representation of the orographic features. The GEOS-1 atmospheric model supplies its own topography. It is derived from an averaging of a Navy 10 minute by ten minute dataset supplied by the National Center for Atmospheric Research (NCAR). The averaged topography was passed through a Lanczos filter in both dimensions to remove the smallest scales (Takacs, Molods, and Wang, 1994).

The geographic global distribution of orographic pressure torque at a specific time is displayed in Fig. 4.2.1. Notable features of the Fourier analysis include greater relative concentration of power in the subdaily range for the zonal component, led by a half-daily mode. All three components show most of the power in modes with periods under 15 days, i.e., 80.2% (x), 80.6% (y), and 85% (z). Seasonal variability is approximately four times greater in equatorial components than in the zonal. Curiously, the x-component annual variability is much larger than the y-component counterpart, due to the mode with period of 357.5 days. Geographically, the x-component shows greater variability in the Andes and Himalayas, at least for the particular epoch shown in Fig. 4.2.1. Modes with multiannual periods are prominent in the spectrum for the equatorial components.

4.3. Pressure Torque due to Polar Flattening.

Polar flattening constitutes the largest topographic feature on the surface of the Earth. The ellipticity of figure can be expressed as a function of the colatitude and the flattening parameter "f" by well known relations. Let,

a = 6,378,388 m, (equatorial radius of ellipsoid of .revolution).

f = 1/297, (polar flattening).

H_e : polar ellipticity of figure.

$$H_e = -a \left[f (\cos\theta)^2 + (3/2) f^2 (\cos\theta)^2 - (3/2) f^2 (\cos\theta)^4 \right] + O(f^3)$$

It can be shown that,

$$\partial H_e/\partial\theta = a \left[f \sin 2\theta - (3/4) f^2 \sin 4\theta \right]$$

The atmospheric pressure torque per unit area is then,

$$\mathbf{r} \times (-p_s \mathbf{n}) = -p_s \left[(\partial H_e/\partial\theta) \sin\lambda \mathbf{I} - (\partial H_e/\partial\theta) \cos\lambda \mathbf{j} \right]$$

Note that there is no zonal component due to polar flattening. The global geographic distribution of pressure torque due to polar flattening at a specific time is presented in Fig. 4.3.1.

The pressure torques due to polar flattening are the largest in the atmospheric torque budget, it is pertinent to consider the contributions due to ocean surfaces in the context of the oceanic transfer function to the solid Earth. Assuming isostatic oceanic adjustment for forcing modes with periods greater than 15 days, the atmospheric torque transmitted to the solid Earth is then the sum of the direct torque on the land masses, and part of the ocean torque. The power in modes with periods longer than 15 days is between 31 and 32 percent of the total polar flattening pressure torque, for each of the equatorial components. The single most powerful mode has a period of 361.2 days, both for ocean and land contributions. Daily and semidaily modes appear as second and third in rank for the y-component due to land.

4.4. Pressure Torque due to Equatorial Ellipticity.

The Earth's figure can be approximated by a triaxial ellipsoid, i.e., an equatorial cross section is not perfectly circular, but elliptical. The equatorial ellipticity is much smaller than the polar, but it creates a topographic feature which produces a pressure torque.

The expression for the equatorial ellipticity is similar to that for the polar flattening. Let,

$\beta = \lambda + \lambda_0$

λ : longitude.

λ_0 : Greenwich longitude of major axis of equatorial ellipse.

h : equatorial flattening.

E_e : equatorial ellipticity of figure.

$E_e = -a \left[h (\sin \beta)^2 + (3/2) h^2 (\sin \beta)^2 - (3/2) h^2 (\sin \beta)^4 \right] + O(h^3)$

It can be shown that,

$\partial E_e/\partial\lambda = - a \left[h \sin 2(\lambda + \lambda_0) - (3/4) h^2 \sin 4(\lambda + \lambda_0) \right]$

The atmospheric pressure torque per unit area is then,

$$\mathbf{r} \times (-p_s \mathbf{n}) = -p_s \left[(\partial E_e/\partial\lambda) \cot\theta \cos\lambda \mathbf{I} + (\partial E_e/\partial\lambda) \cot\theta \sin\lambda \mathbf{j} - (\partial E_e/\partial\lambda) \mathbf{k} \right]$$

Note that equatorial ellipticity produces equatorial and zonal components of torque. The values adopted here for the equatorial flattening "h" and the orientation of the major axis "λ_0" are those associated with the GEM-T2 geopotential model, as given by Bursa and Pec (1993), i.e.,

$\lambda_0 = - 14.94°$

$h = 1/91470$

The global geographic distribution of pressure torque due to equatorial ellipticity at a specific time is presented in Fig. 4.4.1. The Fourier analysis shows most of the power in modes with periods under 15 days. The single most powerful mode, however, is in the annual range, with a period of 361.2 days. The zonal component exhibits greater variance in the subdaily range, with daily and semidaily modes prominent for both ocean and land contributions.

5. Gravitational Torque.

Dehant et al. (1996) show that the gravitational torque produced by the atmosphere on the solid Earth can be approximated by the following expression,

$$\Gamma_g = - \int_S p_s (\mathbf{r} \times \mathbf{n}_{grav}) \, dS$$

where,

$\mathbf{n}_{grav}$: unit vector normal to the equipotential surface, directed toward the center of the Earth.

S : surface of the Earth

It is assumed that the surface pressure is only a function of the weights of the air columns, and that the vectors $\mathbf{r}$ and $\mathbf{n}_{grav}$ do not vary throughout the height of the atmosphere.

The gravitational field used in the computations is EGM96, the Earth Gravitational Model 1996 (EGM96) was developed in collaboration by the NASA Goddard Space Flight Center (GSFC), the National Imagery and Mapping Agency (NIMA), and The Ohio State University (OSU). It is a spherical harmonic model of the Earth's gravitational potential to degree 360. It incorporates surface gravity data, altimeter-derived gravity anomalies, extensive satellite tracking data, and direct altimeter ranges. For a detailed description of the model see Lemoine et al., 1998.

Note that the direction of $\mathbf{n}_{grav}$ is opposite to that of $\mathbf{n}$ in section 4, i.e., the gravitational torque acts in opposition to the pressure torque.

Most of the gravitational torque power is associated with the equatorial components. All three components have over 68% of the variance in the high frequency range. The zonal component has greater relative power concentration in the subdaily range (daily and half-daily modes). The equatorial components most powerful modes have periods of 357.5 and 381.3 days.

6. Total Torque.

The total atmospheric torque on the oceans and solid Earth is obtained from the sum of the individual components : wind stress torque, pressure torque, and gravitational torque. The resulting time series are displayed in Fig. 6.1. Power spectra are shown in Fig. 6.2. The results of the Fourier analysis are presented in Table 6.1.

The results for the total torque show equatorial components which are seven times as powerful as the zonal. Most of the power occurs at the high frequency end of the spectrum, modes with periods less than 15 days account for 67%, 67.5%, and 83.9% of the power in the x, y, and z components respectively. The single most powerful modes, however, are close to annual, with periods of 357.5 and 381.3 days. The zonal component has greater concentration of power in the subdaily range, with one semidaily mode in fourth rank.

Each of the various torques has a mean value and a time varying part, the analysis has dealt only with the latter. Table 6.2 presents the mean values for the torques, as well as the algebraic sum total.

The total torque acting on the atmosphere is equal in magnitude and of opposite sign to that acting on the ocean and solid Earth. Furthermore, this torque is related to the time rate of change of atmospheric angular momentum (h_x, h_y, h_z) by the well known relations,

$$\Gamma_x = dh_x/dt - \Omega_z h_y$$

$$\Gamma_y = dh_y/dt + \Omega_z h_x$$

$$\Gamma_z = dh_z/dt$$

It is possible to perform the angular momentum calculations for the atmosphere to compare with the torque values. However, it would be only an internal test of the model. The gravitational field model used to compute the gravitational and marine geoid torques was not used in the development of the atmospheric model, this will undoubtedly lead to discrepancies. However, it is of interest to check on the large mean value obtained for the x-torque component. The mean value for the term dh_x/dt is small and can be neglected. The

term $\Omega_z h_y$ has been computed and is shown in Fig. 6.3, where the two time series correspond to matter terms computed with and without the inverted barometer effect, as done by Chao and Au (1991). The mean values obtained are 1950.39 H for the case without IB effects, and 1807.64 H for the IB case. No special significance is attributed to the closeness of the second value to the one using the torque approach, it is probably coincidental. However, these results indicate the possible existence of a large mean value for the x-component of the torque. What could be the physical source? According to M. J. Bell (1994), an important contributor is the Siberian high pressure system, which is not balanced and which produces a torque on the Earth's bulge. The values shown in Table 6.2, however, indicate that the main contribution is due to polar flattening pressure torque over water.

The existence of atmospheric torque modes with periodicities near that of the Chandler wobble is worth noticing. The x-component of total torque exhibits two modes in third and fourth rank, with periodicities of 408.6 and 476.7 days, each with power in excess of 28 H. In addition, there is a mode with period of 440.0 days and 13.31 H power, ranked 20th. These three modes also appear in the spectrum for the y-component: 408.6 days (16.58 H), 476.7 days (9.89 H), and 440.0 days (3.54 H). Examination of the various spectra finds these modes only in torques associated with the pressure field: the orographic, marine geoid, and gravitational. However, they are not found in the spectra of polar flattening or equatorial ellipticity pressure torques. A possible explanation: they result from the interaction of the pressure field with spatial wavelengths of higher degree than are found in the triaxility of the Earth's figure. The strongest contributions come from the gravitational torque: the spectrum for the x-component shows the 476-day mode (27.8 H), the 408-day mode (27.6 H), and the 440-day (11.3 H), the y-component exhibits the 408-day mode (16 H).

7. Summary.

The **GEOS-1** general circulation model has been used to compute atmospheric torques on the oceans and solid Earth for the period 1980-1995. The time series for the various torque components have been analyzed by means of Fourier transform methods.

It was determined that the wind stress torque over land is more powerful than the wind stress torque over water by 55.1%, 41.5%, and 79.9% for the x, y, and z components respectively. This is mainly the result of power in the high frequency range. The ocean wind stress torque equatorial components, however, have greater variance in the seasonal range. Marine wind friction torques are more important also in the interannual range. Annually, the ocean is the main contributor to zonal variability, driven by one single mode with period of 361.2 days. Adding the marine and land contributions yields the total torque due to wind stress. The total equatorial components exceed the zonal total by 22.4%.

The pressure torques due to polar flattening, equatorial ellipticity, marine geoid, and continental orography were computed.

The orographic or "mountain torque" components are more powerful than their wind stress counterparts (land plus ocean) by 231% (x), 191% (y), and 77% (z). The main contributors to this difference are found in modes with periods in the 1-15 days range. The wind stress (9.46 Hadleys) contributes more to the annual variability of the zonal component than the mountain torque (3.07 Hadleys). The contributions to the seasonal zonal variability are about equal, 3.02 Hadleys for wind stresses and 3.91 Hadleys for the mountain torque. The zonal contributions with periods over 370 days yield 8.47 Hadleys due to wind stresses and 7.67 Hadleys in the mountain torque budget. The orographic equatorial contributions are more powerful than those due to wind stress throughout the entire spectrum.

The marine pressure torques due to geoidal undulations are much smaller than the orographic ones, as expected. They are only 2.77% (x), 3.56% (y), and 5.24% (z) of the corresponding mountain torques. The geoidal pressure torques are approximately equal in magnitude to those produced by the equatorial ellipticity of the Earth. Their power distributions as a function of period length are also similar. There is a difference in the annual contributions to the

zonal component, that of the equatorial ellipticity is 4.5 times larger, mainly the result of a mode with a period of 361.2 days. Marine geoid pressure torques contribute the single largest zonal mean value.

The pressure torque due to polar flattening makes the largest contributions to the atmospheric torque budget. It has no zonal component, only equatorial ones. Most of the power of the latter, between 68% and 69%, is found in modes with periods under 15 days. The single most powerful mode has a period of 361.2 days.

The gravitational torque ranks second in power only to the polar flattening pressure torque. Unlike the former, it does produce a zonal component, albeit much smaller (0.86%, 0.88%) than the equatorial ones. The gravitational and pressure torques have opposite signs, therefore, the gravitational torque nullifies 42.34% (x), and 42.67% (y), of the total pressure torque. Zonally, however, the gravitational torque amounts to only 6.28% of the total pressure torque. The gravitational torque also nullifies 47.32% of the mean polar flattening x-torque component.

The power budget for the total atmospheric torque yields 7595 and 7120 Hadleys for the equatorial components and 966 Hadleys for the zonal. The x-component exhibits a large mean value (1811 H), mainly the result of polar flattening pressure torque acting on the ocean surfaces. Atmospheric torque modes with periods of 408, 440, and 476 days appear in the spectrum of the equatorial components.

Finally, a word of caution concerning the values presented for the various torques. The numerical calculations involve uncertain quantities and subtraction of large numbers. The associated error bounds could be large.

Tables

	X	Y	Z
Wind Stress			
Water	231.860	244.179	172.398
Land	359.660	345.605	310.187
Pressure			
Polar Flattening	14387.6	14144.1	
Equatorial Ellipticity	61.0054	58.8186	54.0057
Marine Geoid	54.3629	61.2244	44.9128
Orography	1959.07	1719.57	855.970
Gravitational	6970.18	6820.76	60.0249
Total	7595.44	7120.57	966.460

Table 6.1. Total power (Hadleys) for various torque components.

	X	Y	Z
Wind Stress			
Water	-7.91	8.36	0.55
Land	-1.52	-1.57	3.18
Pressure			
Polar Flattening			
Land	-31094.0	24634.5	
Water	34915.7	-24635.1	
Land and Water	3821.89	-0.44	
Equatorial Ellipticity	27.51	-1.08	4.91
Marine Geoid	-222.67	9.51	54.69
Orography	-1.43	-3.93	-7.32
Gravitational	-1808.59	-42.13	-8.33
Total	1811.34	-33.95	47.83

Table 6.2. Mean values (Hadleys) for various torque components.

References

Amorocho, J., and J. J. DeVries, "A New Evaluation of the Wind Stress Coefficient Over Water Surfaces", Journal of Geophysical Research, Vol. 85, No. C1, pages 433-442, January 20, 1980.

Bell, M. J., "Oscillations in the equatorial components of the atmosphere's angular momentum and torques on the earth's bulge", Q. J. R. Meteorol. Soc., Vol. 120, pages 195-213, 1994.

Boer, G. J., "Earth-Atmosphere Exchange of Angular Momentum Simulated in a General Circulation Model and Implications for the Length of Day", Journal of Geophysical Research, Vol. 95, No. D5, Pages 5511-5531, April 20, 1990.

Bryan, F. O., "The axial angular momentum balance of a global ocean general circulation model", Dynamics of Atmospheres and Oceans, Vol. 25, pages 191-216, 1997.

Bunker, A. F., "Computations of Surface Energy Flux and Annual Air-Sea Interaction Cycles of the North Atlantic Ocean", Monthly Weather Review, Vol 104, pages 1122-1140, September 1976.

Bursa, M. and Karel Pec, Gravity Field and Dynamics of the Earth, Springer-Verlag, New York, 1993.

Chao, B. F., and A. Y. Au, "Atmospheric Excitation of the Earth's Annual Wobble: 1980-1988", Journal of Geophysical Research, Vol. 96. No. B4, pages 6577-6582, April 10, 1991.

Cressman, G. P., "Improved Terrain Effects in Barotropic Forecasts", Monthly Weather Review, pages 327-342, September-December 1960.

Dehant, V., Ch. Bizouard, J. Hinderer, H. Legros, and M. Greff-Lefftz, "On atmospheric pressure perturbations on precession and nutations". Physics of the Earth and Planetary Interiors, 96: 25-39, 1996.

Garratt, J. R., "Review of Drag Coefficients over Oceans and Continents", Monthly Weather Review, Vol. 105, pages 915-929, July 1977.

Large, W. G., and S. Pond, "Open Ocean Momentum Flux Measurements in Moderate to Strong Winds", Journal of Physical Oceanography, Vol. 11, pages 324-336, March 1981.

La Valle, L., and P. D. Girolamo, "Determination of the geostrophic drag coefficient", Tellus XXVII, 1, pages 87-92, 1975.

Ponte, R. M., "Variability in a homogeneous global ocean forced by barometric pressure". Dynamics of Atmospheres and Oceans, 18: 209-234, 1993.

Rosen, R. D., "The Axial Momentum Balance of Earth and its Fluid Envelope", Surveys in Geophysics 14: 1-29, 1993.

Schubert, S. D. , W. Min, L. Takacs, and J. Joiner, "Reanalysis of Historical Observations and its Role in the Development of the Goddard EOS Climate Data Assimilation System", Adv. Space Res., Vol. 19, No. 3 : 491-501, 1997.

Segschneider J., and J. Sundermann, "Response of a Global Ocean Circulation Model to Real-Time Forcing and Implications to Earth's Rotation", Journal of Physical Oceanography, Vol. 27, 2370-2380, 1997.

Swinbank, R., "The global atmospheric angular momentum balance inferred from analyses made during the FGGE", Quart. J. R. Met. Soc., Vol 111, pp. 977-992, 1985.

Takacs, L. L., Andrea Molod, and Tina Wang, "Documentation of the Goddard Earth Observing System (GEOS) General Circulation Model-Version 1, NASA Technical Memorandum 104606, Vol. 1, Sept. 1994.

Wahr, J. M., "The effects of the atmosphere and oceans on the Earth's wobble and the seasonal variations in the length of day. I. Theory." Geophys. J. R. Astron. Soc., 70: 349-372, 1982.

Wahr, J. M., and A. H. Oort, "Friction- and Mountain-Torque Estimates from Global Atmospheric Data", Journal of Atmospheric Sciences, Vol. 41, No. 2, pages 190-204, January 1984.

Wu, J., "Wind Stress and Surface Roughness at Air-Sea Interface", Journal of Geophysical Research, Vol. 74, No. 2, January 15, 1969.

— "Wind-Stress Coefficients over Sea Surface near Neutral Conditions- A Revisit", Journal of Physical Oceanography, Vol. 10, pages 727-740, May 1980.

Figure Captions.

Figure 3.1. Geographic distribution of wind stress torque (Hadleys/1000). Epoch: April 1, 1980. a) x-component. b) y-component. c) z-component.

Figure 4.1.1. Geographic distribution of marine geoid pressure torque (Hadleys). Epoch: April 1, 1980. a) x-component. b) y-component. c) z-component.

Figure 4.2.1. Geographic distribution of orographic pressure torque (Hadleys). Epoch: April 1, 1980. a) x-component. b) y-component. c) z-component.

Figure 4.3.1. Geographic distribution of polar flattening pressure torque (Hadleys). Epoch: April 1, 1980. a) x-component. b) y-component.

Figure 4.4.1. Geographic distribution of equatorial ellipticity pressure torque (Hadleys/100). Epoch: April 1, 1980. a) x-component. b) y-component. c) z-component.

Figure 6.1. Total torque (Hadleys). a) x-component. b) y-component. c) z-component.

Figure 6.2. Total torque power spectrum (Amplitude in Hadleys). a) x-component. b) y-component. c) z-component.

Figure 6.3. The term ($\Omega_z h_y$), x-component, time rate of change of atmospheric angular momentum. a) with inverted barometer effects. b) without inverted barometer effects.

TWX 800401 000000

3.1(a)

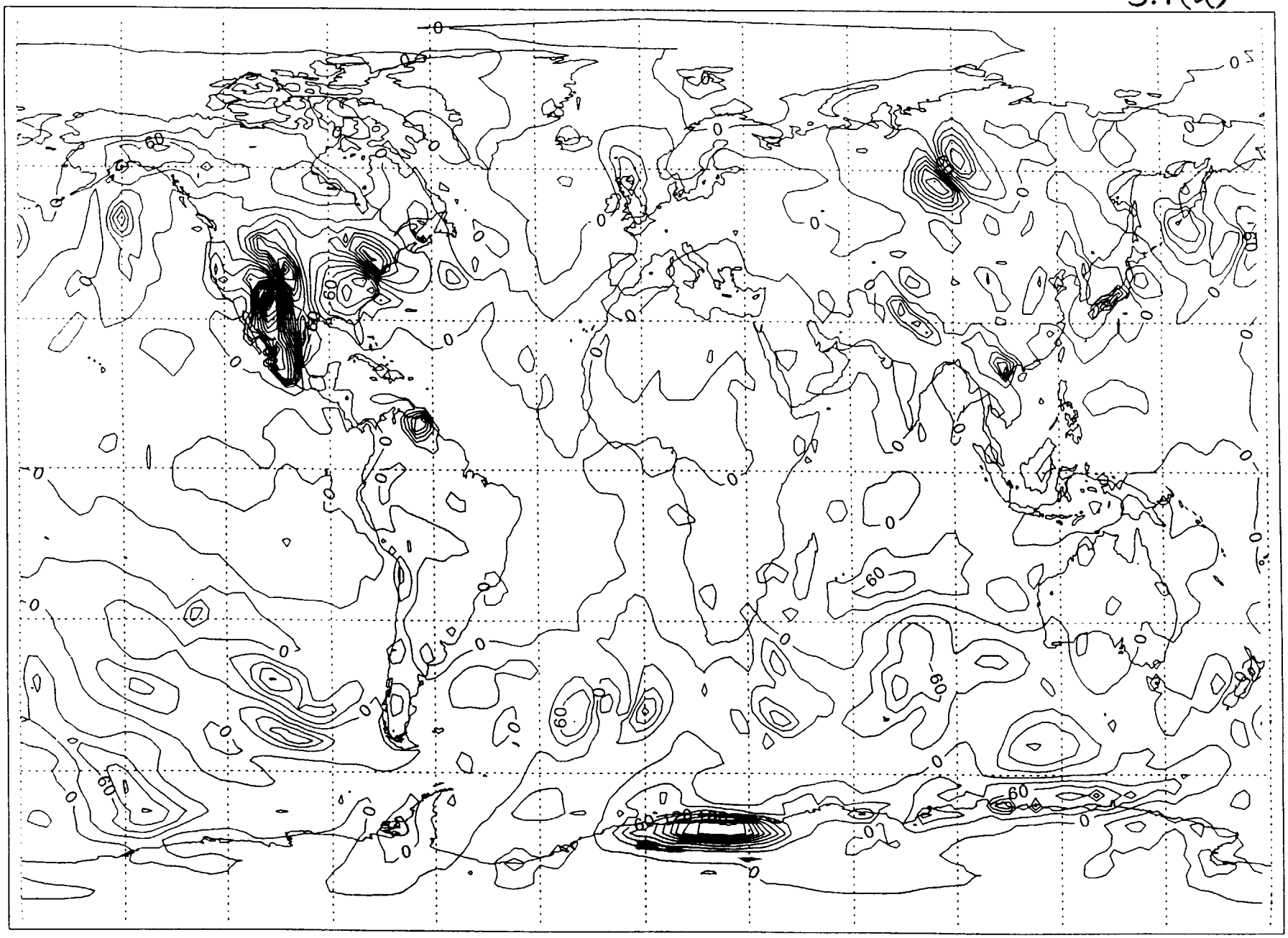

TWY 800401 000000

3.1(b)

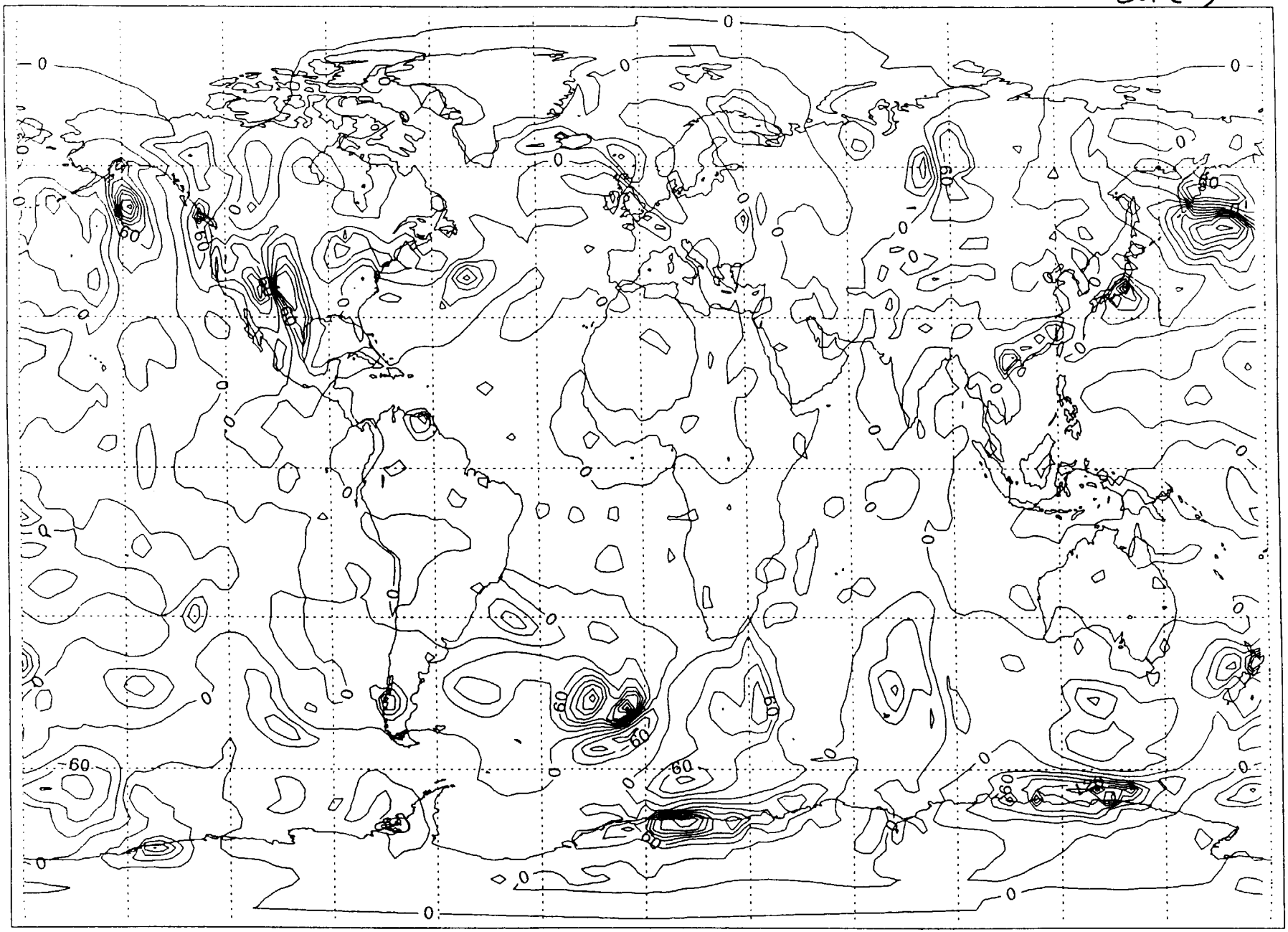

TWZ 800401 000000

3.1(c)

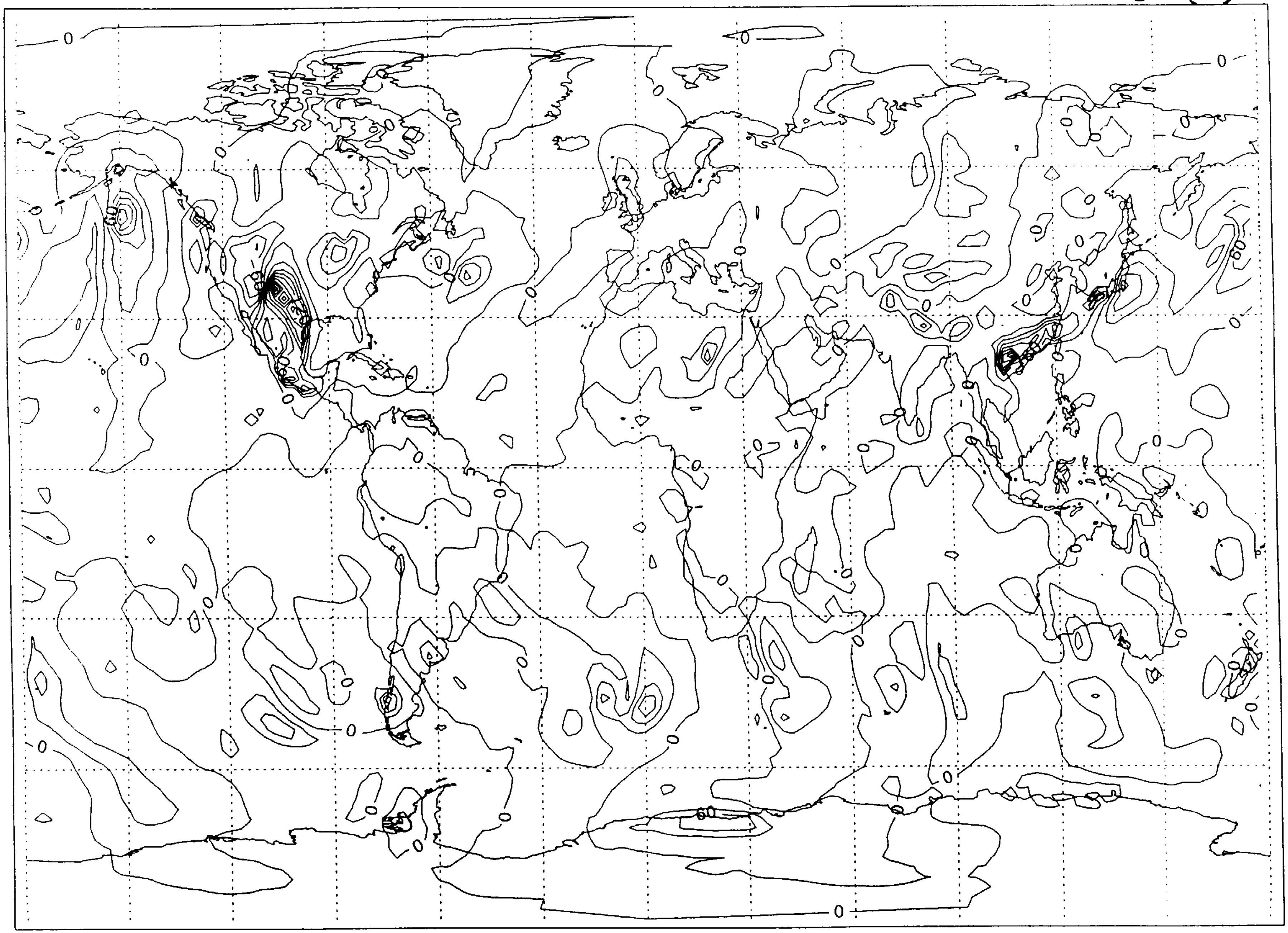

TPX (geoid) 800401 000000

4.1.1 (a)

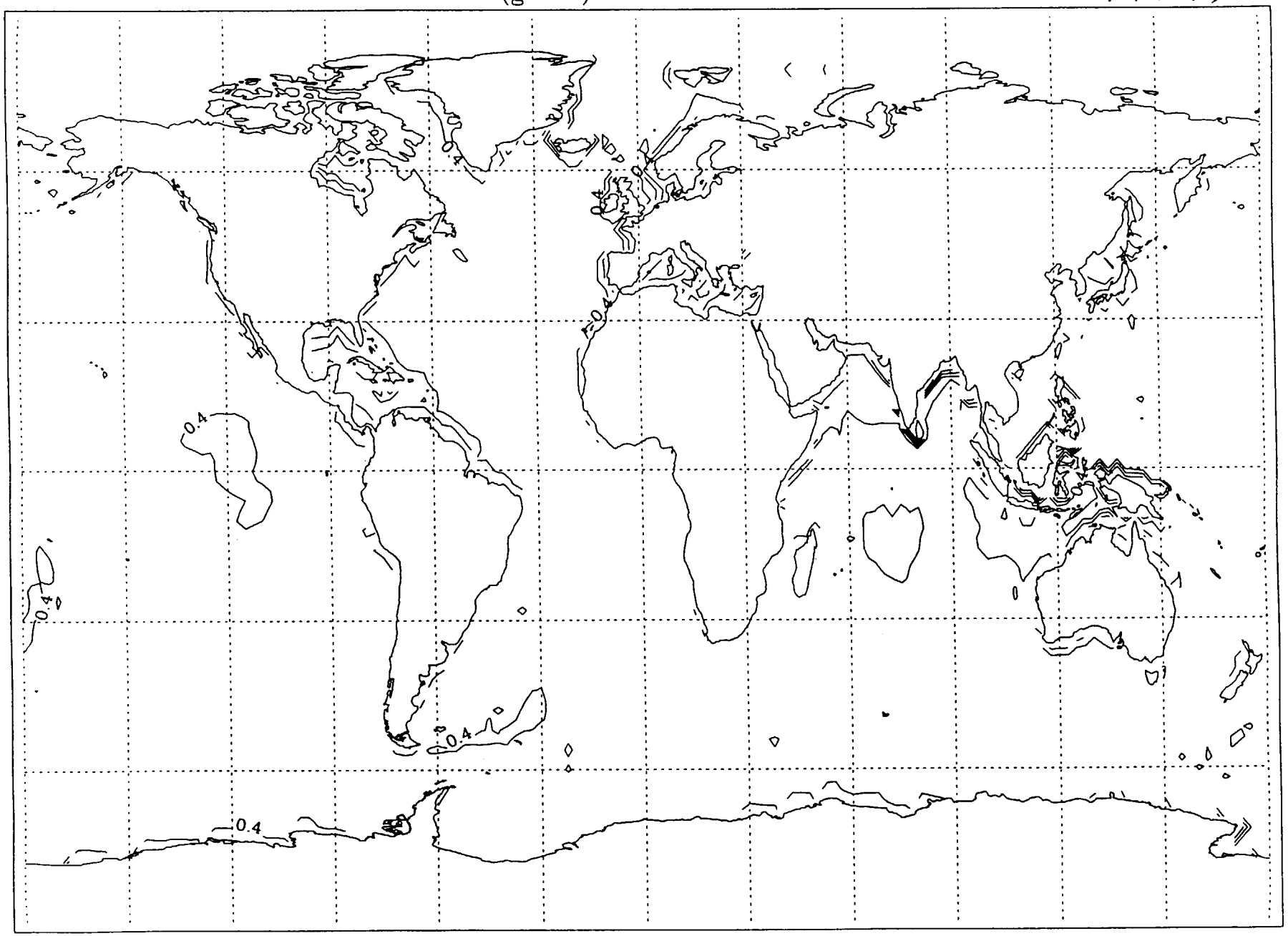

TPY (geoid) 800401 000000

4.1.1 (b)

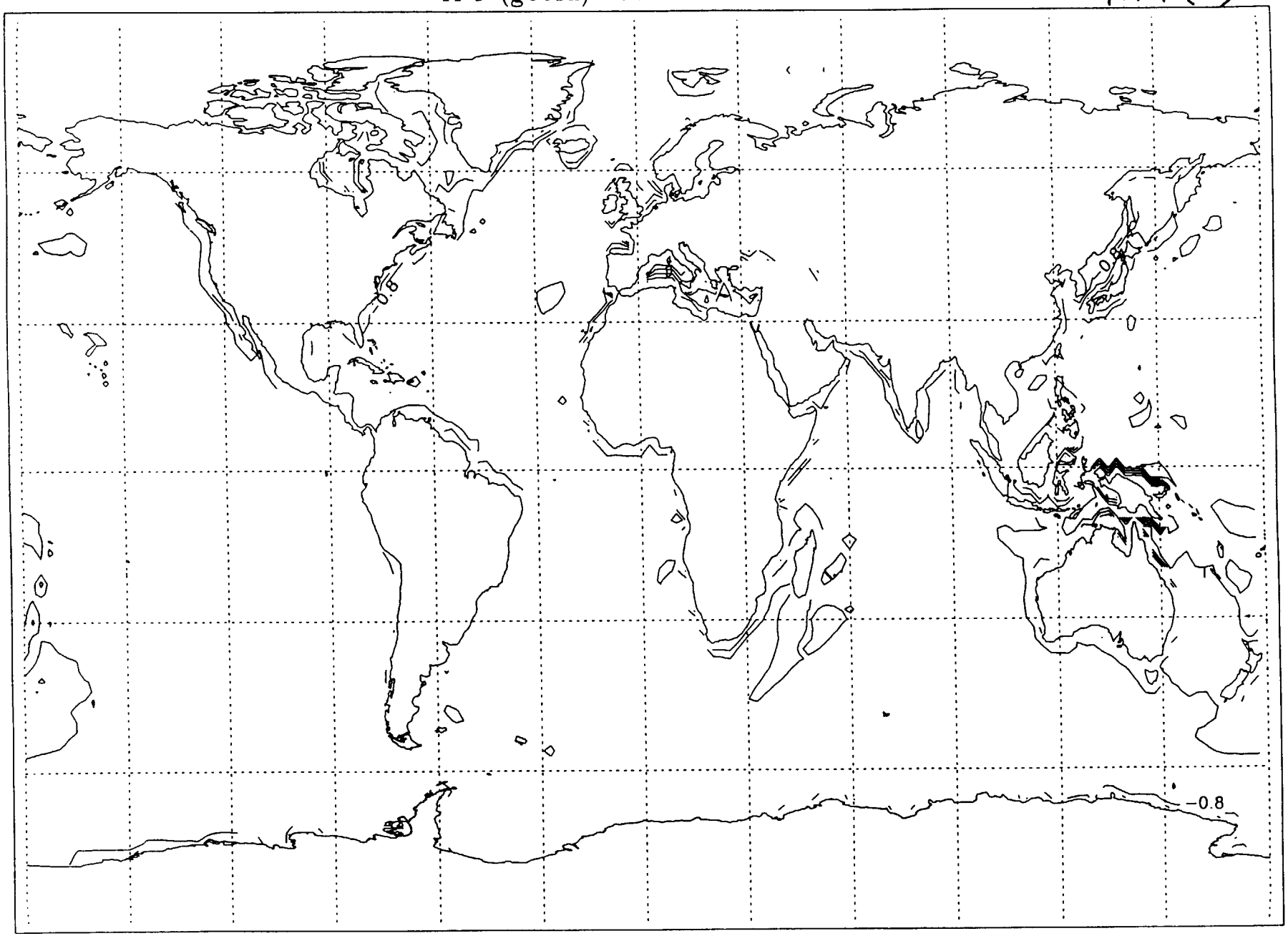

TPZ (geoid) 800401 000000

4.1.1(c)

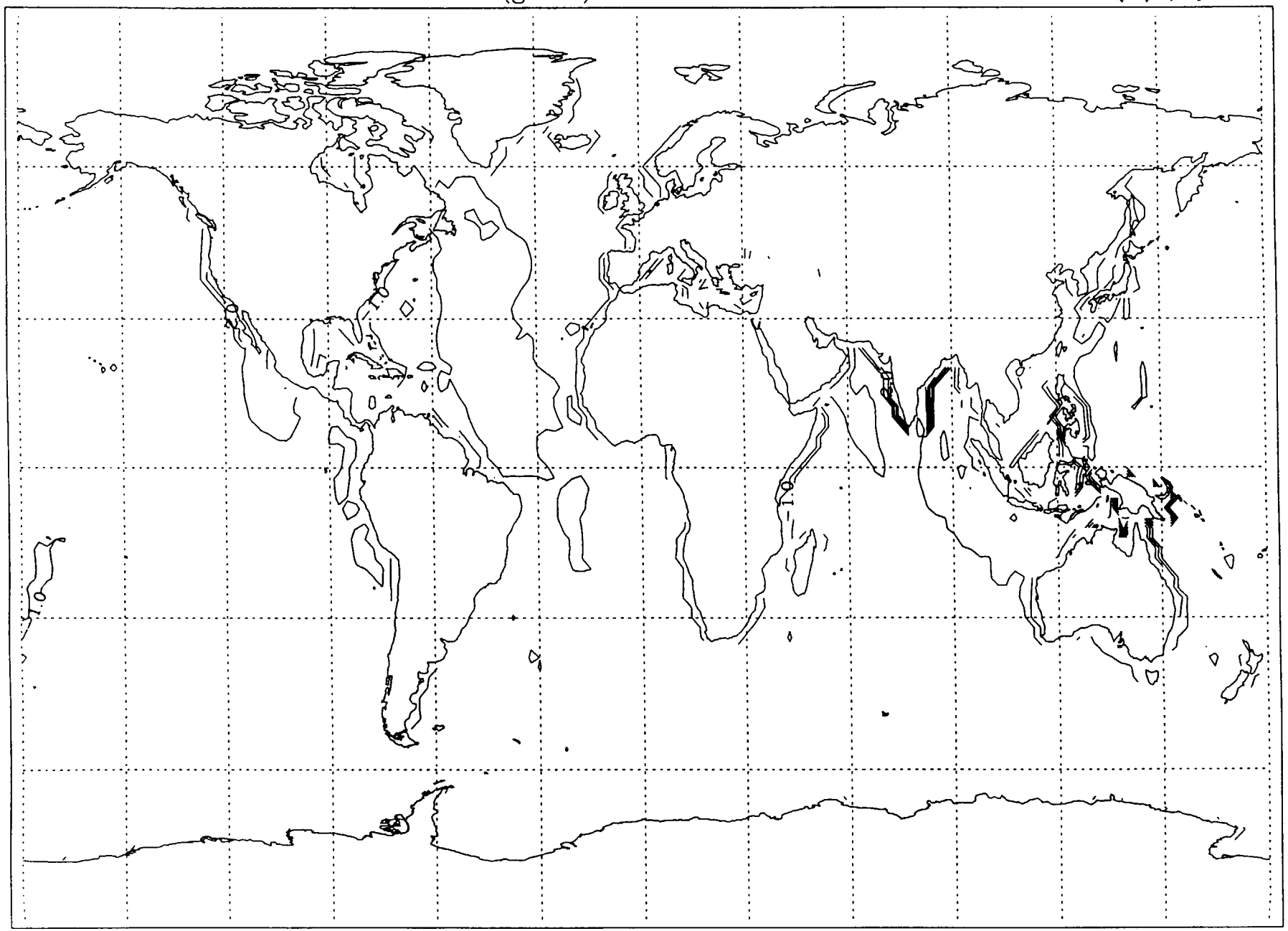

TPX 800401 000000

4.2.1(a)

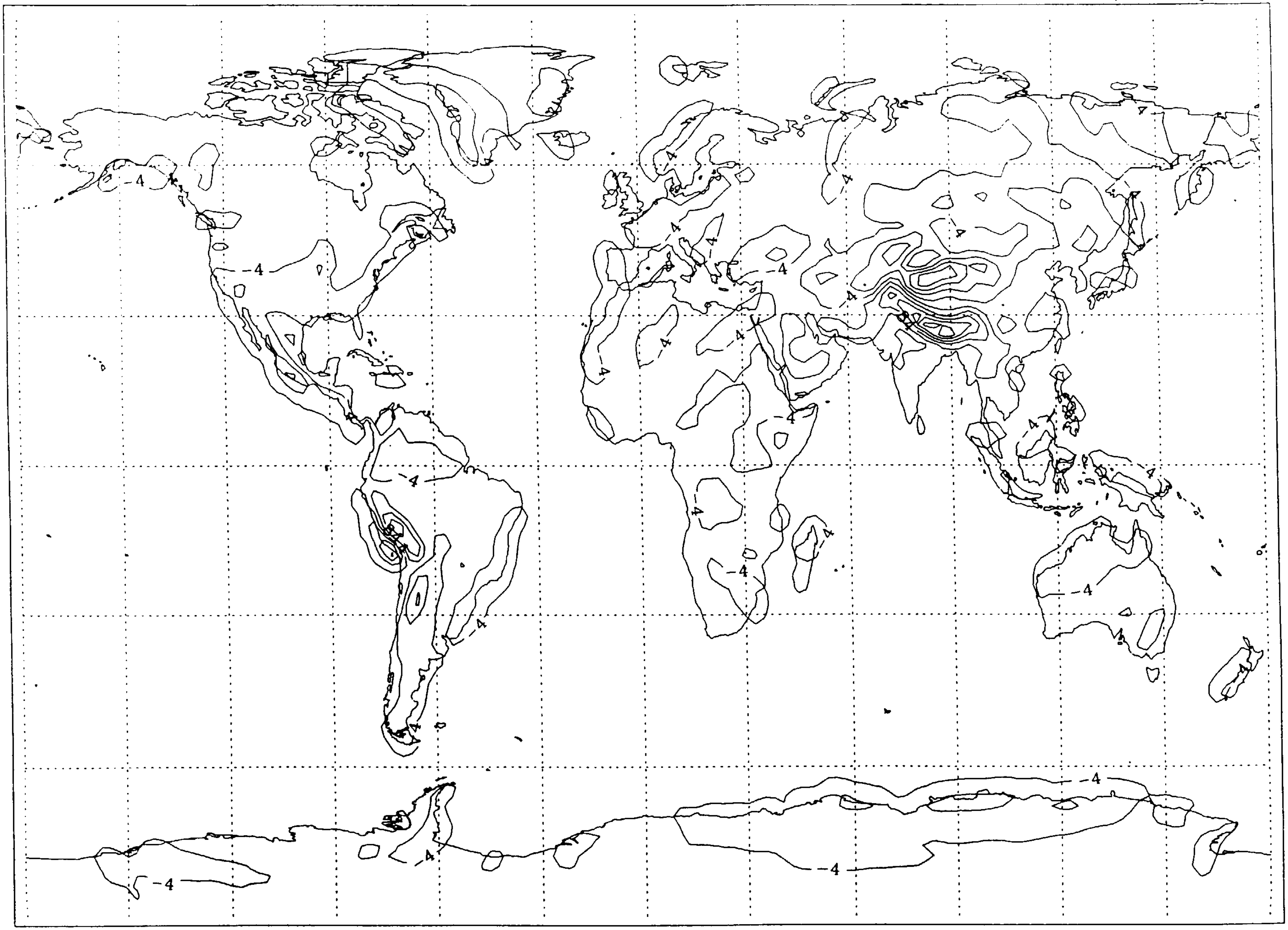

TPY 800401 000000

4.2.1 (b)

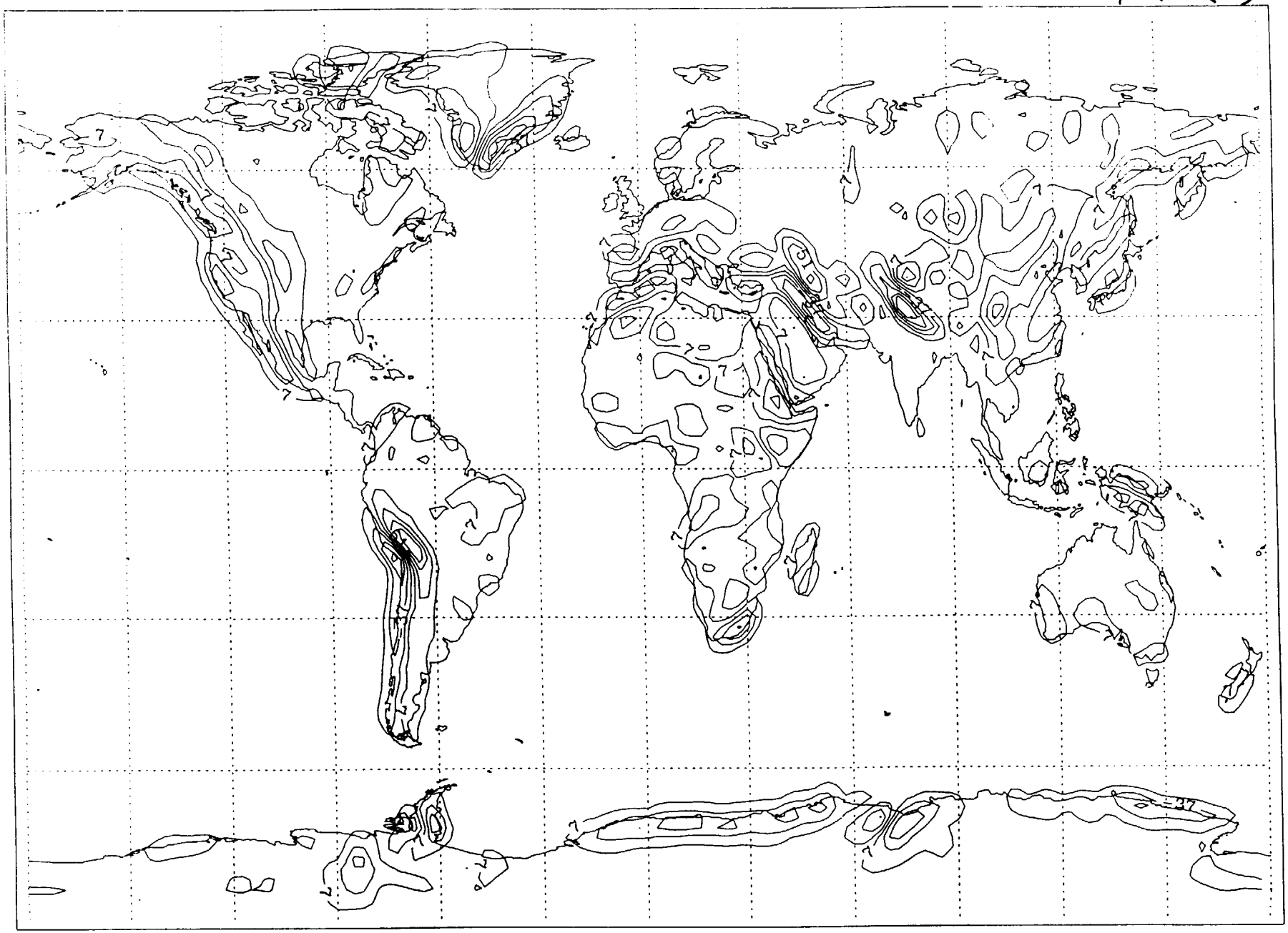

TPZ 800401 000000

4.2.1(c)

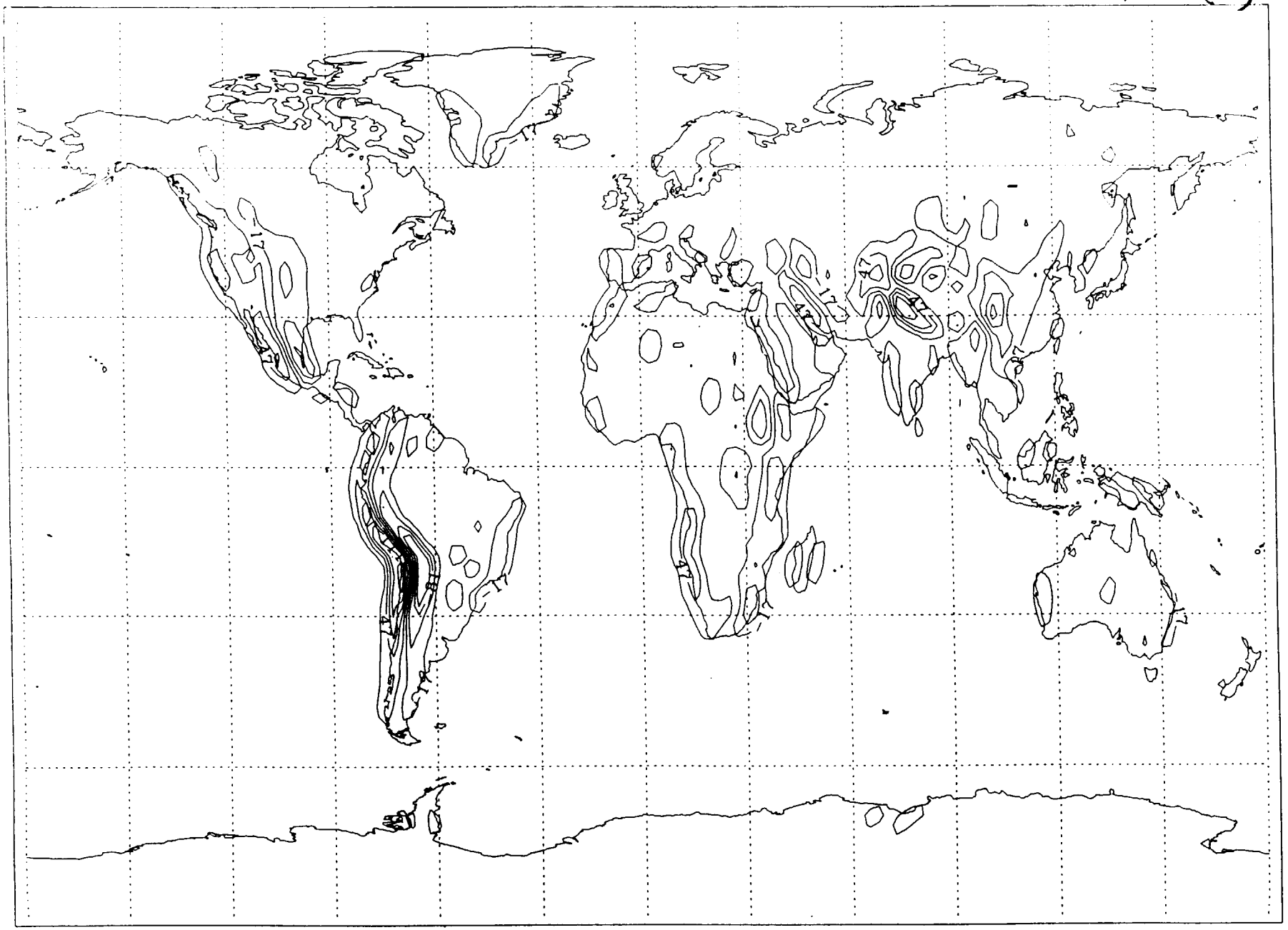

TPEX 800401 000000

4.3.1(a)

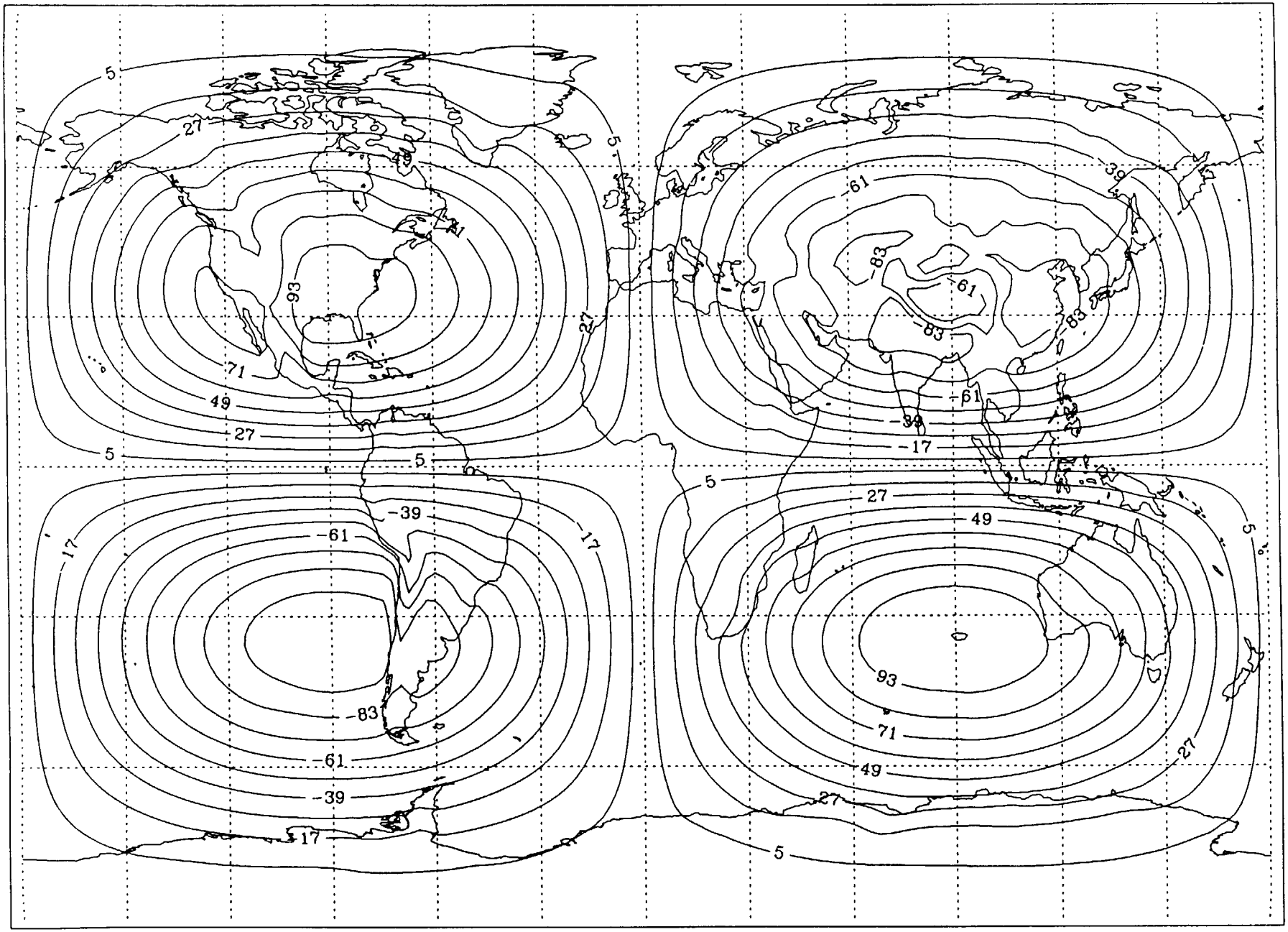

TPEY 800401 000000

4.3.1(b)

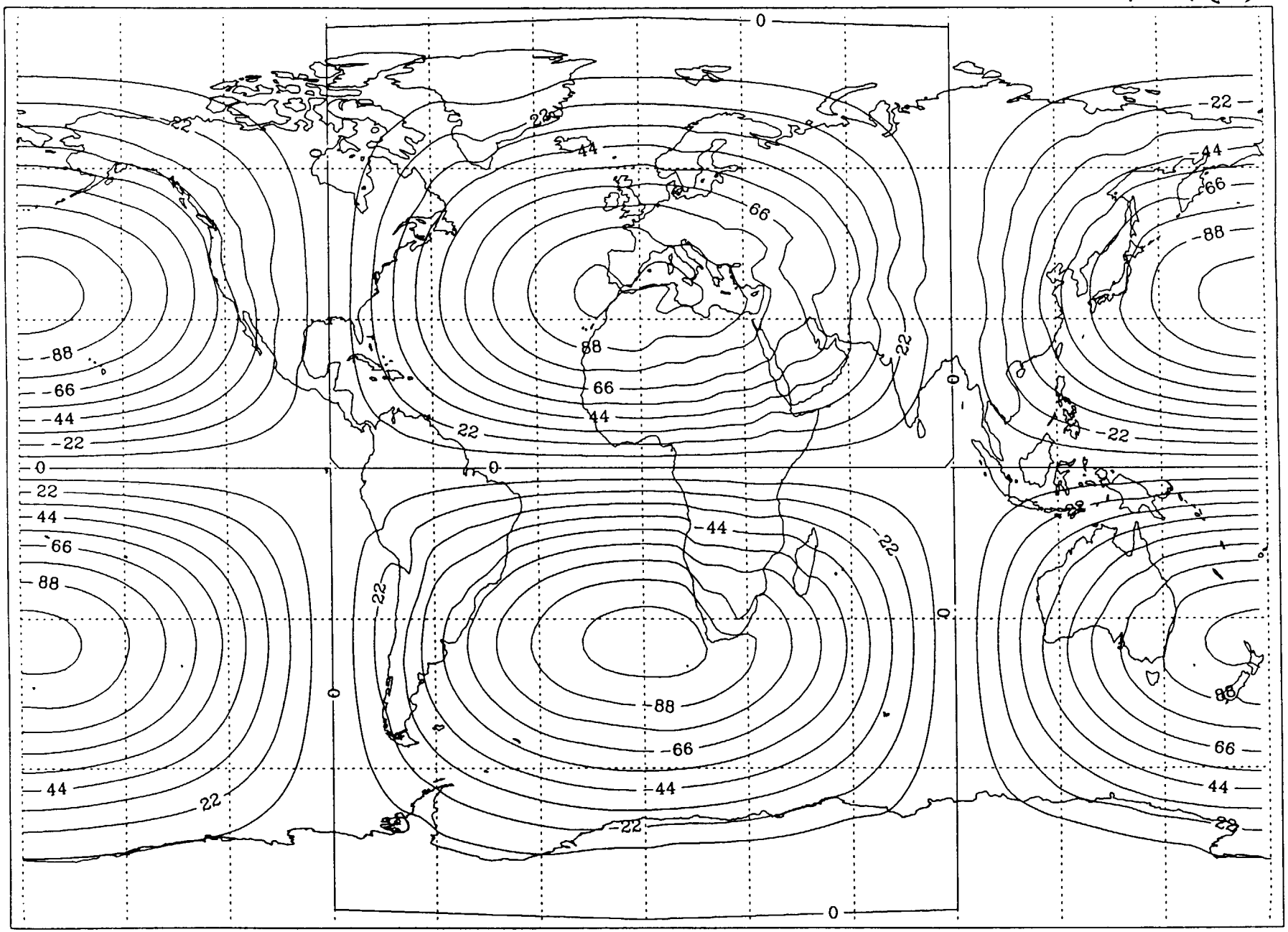

Pressure Torque Equatorial Ellipticity X 800401 000000

4.4.1(a)

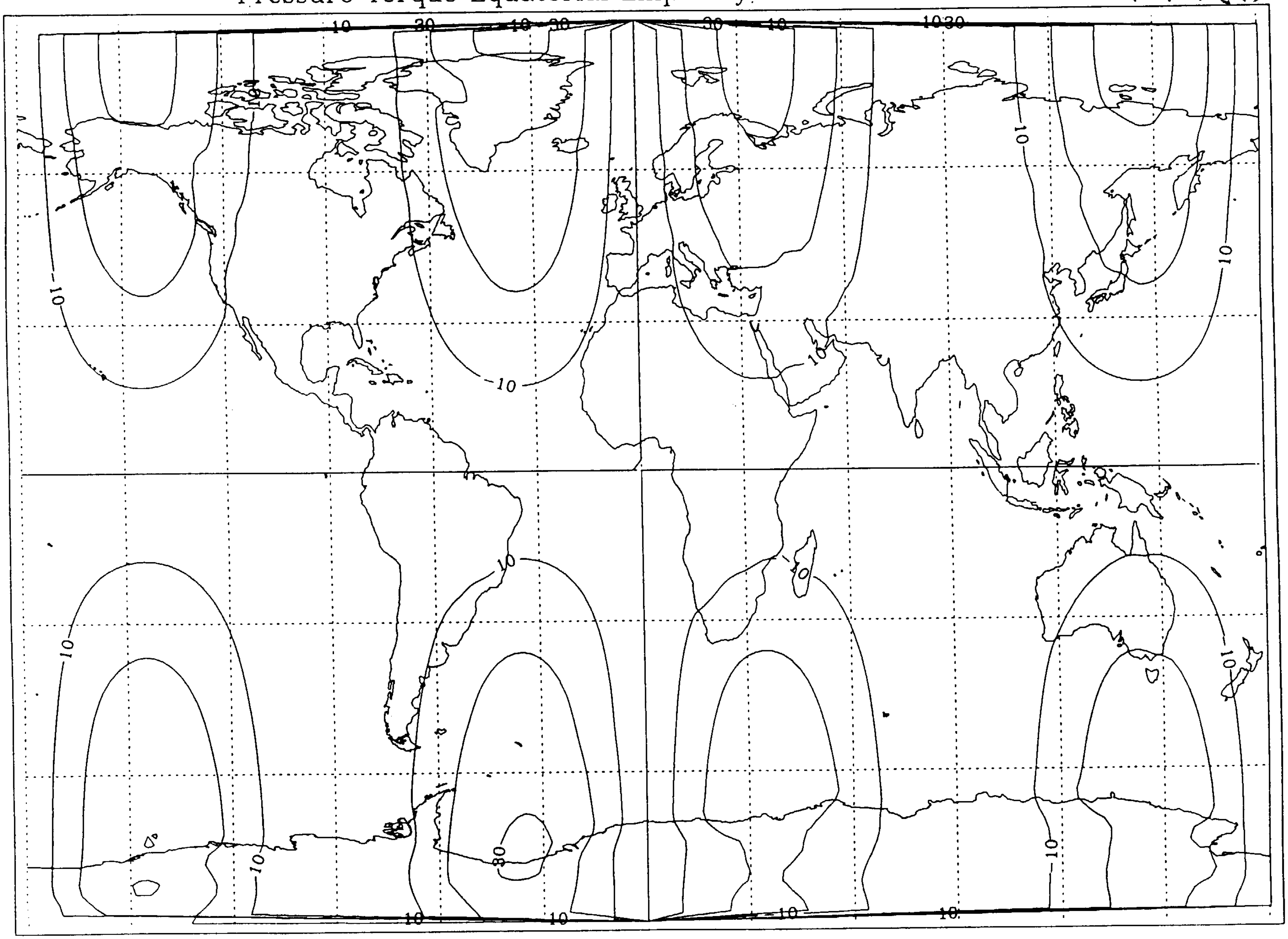

Pressure Torque Equatorial Ellipticity Y 800401 000000 4.4.1(b)

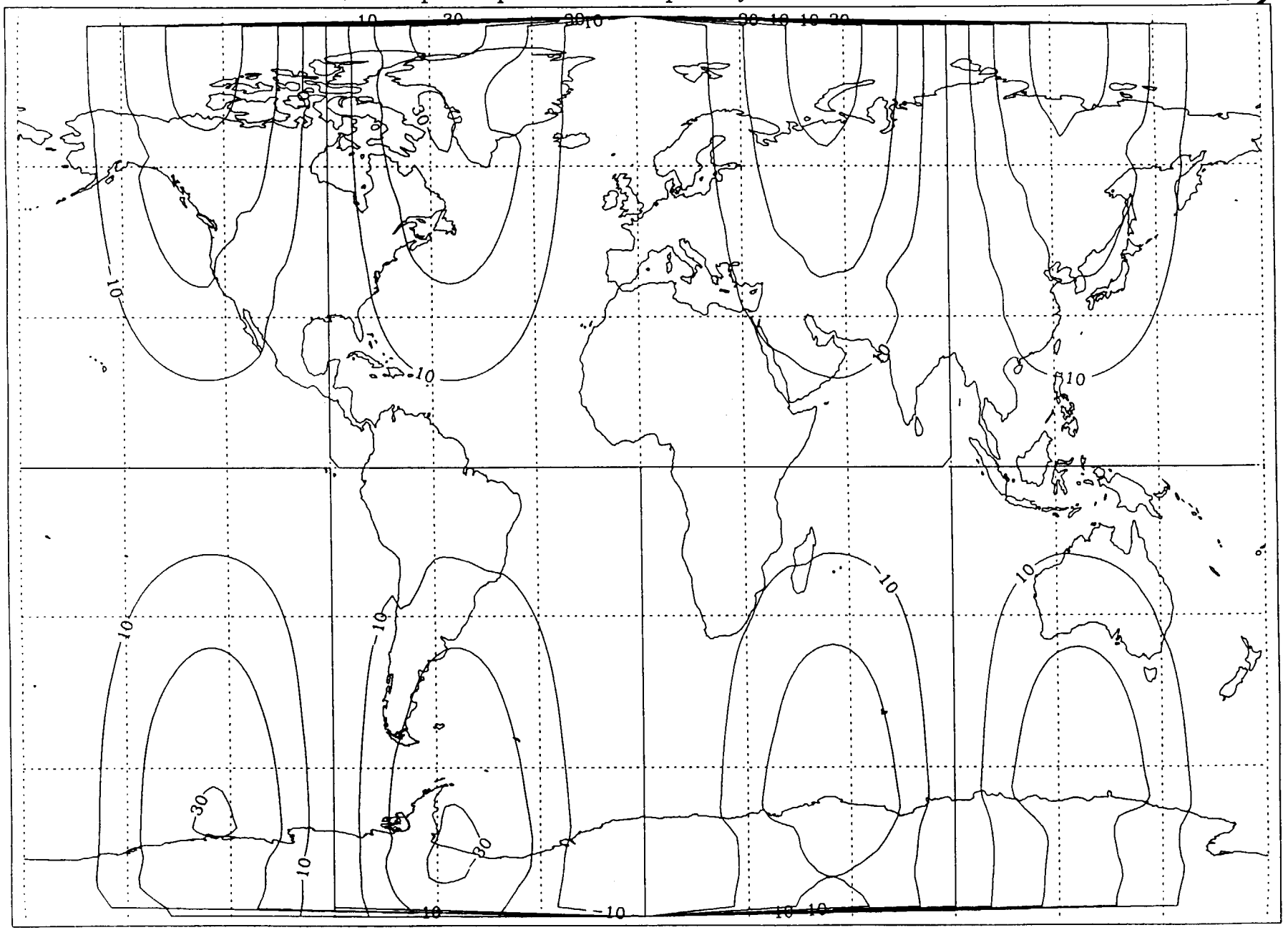

Pressure Torque Equatorial Ellipticity Z 800401 000000

4.4.1 (c)

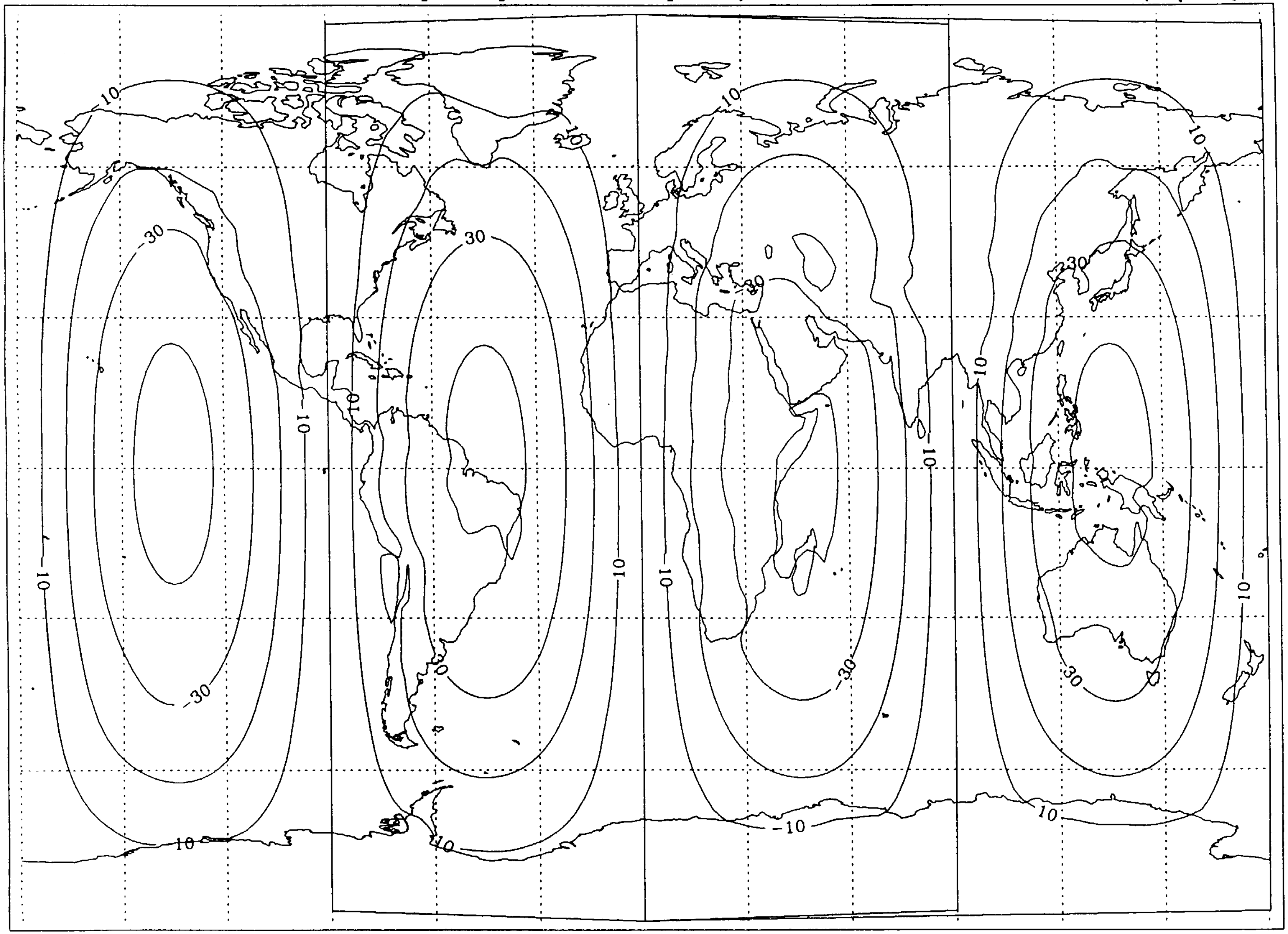

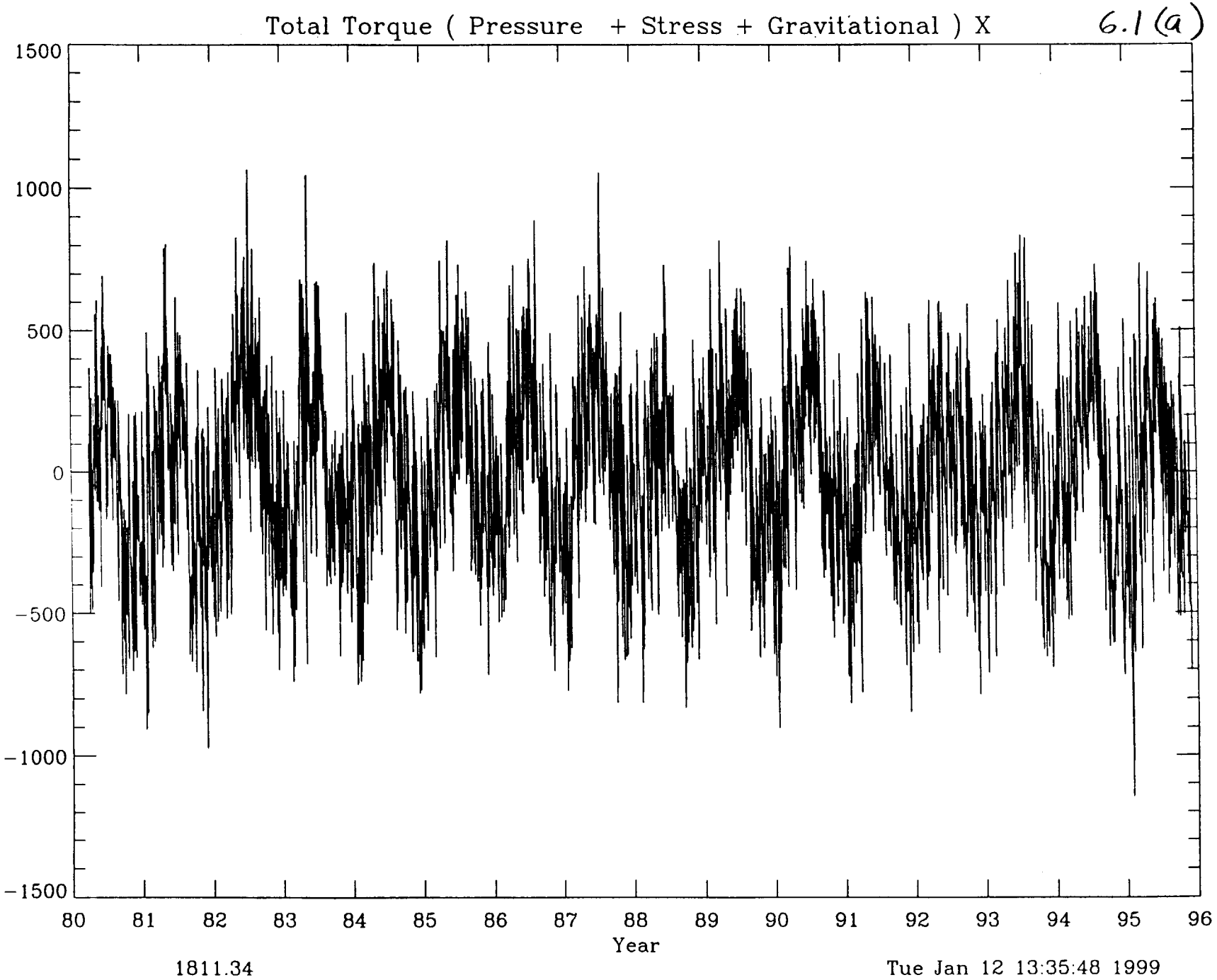
Total Torque (Pressure + Stress + Gravitational) X
6.1 (a)
1500
1000
500
0
−500
−1000
−1500
80
81
82
83
84
85
86
87
88
89
90
91
92
93
94
95
96
Year
1811.34
Tue Jan 12 13:35:48 1999

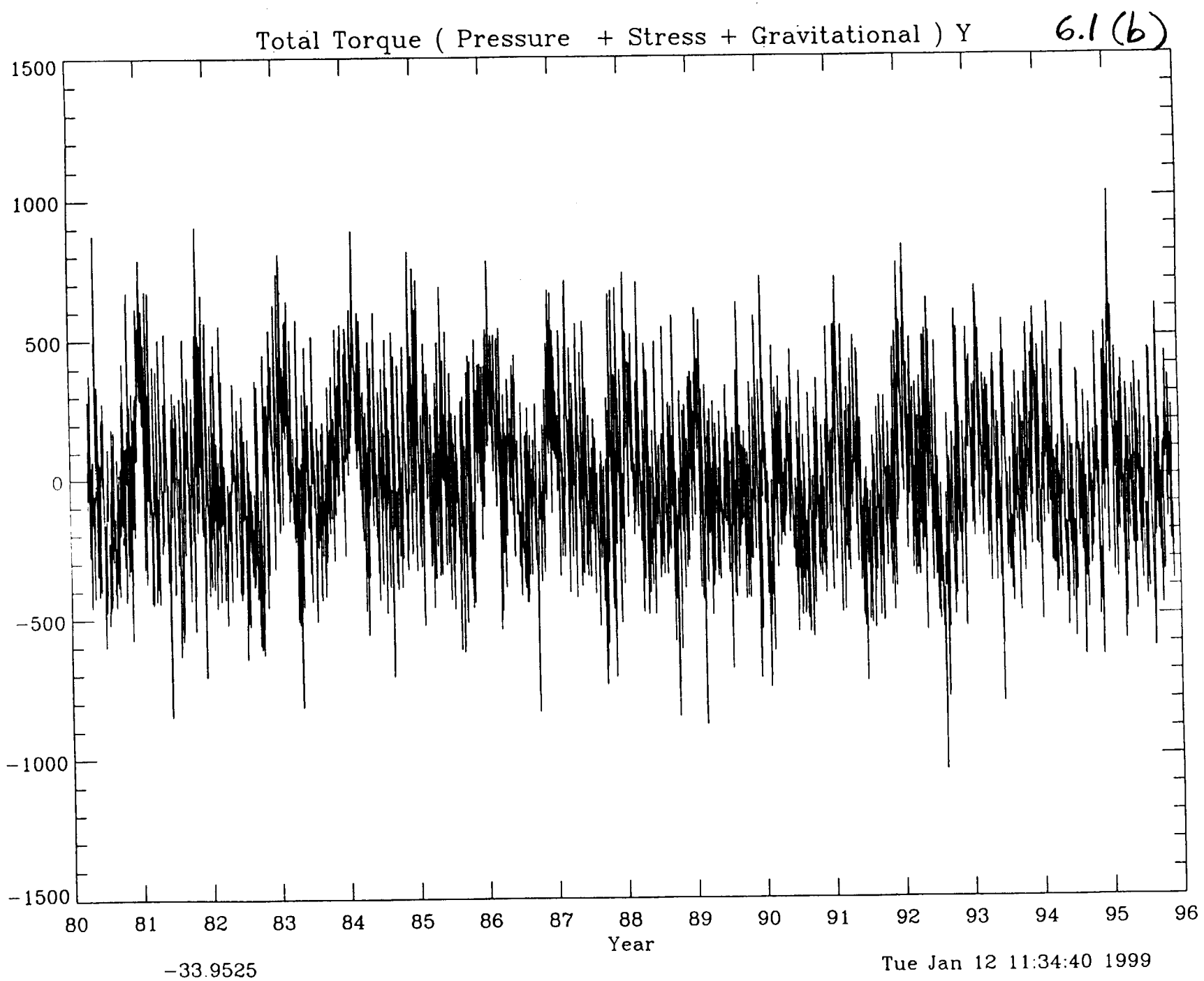
Total Torque (Pressure + Stress + Gravitational) Y
6.1 (b)
1500
1000
500
0
-500
-1000
-1500
80
81
82
83
84
85
86
87
88
89
90
91
92
93
94
95
96
Year
-33.9525
Tue Jan 12 11:34:40 1999

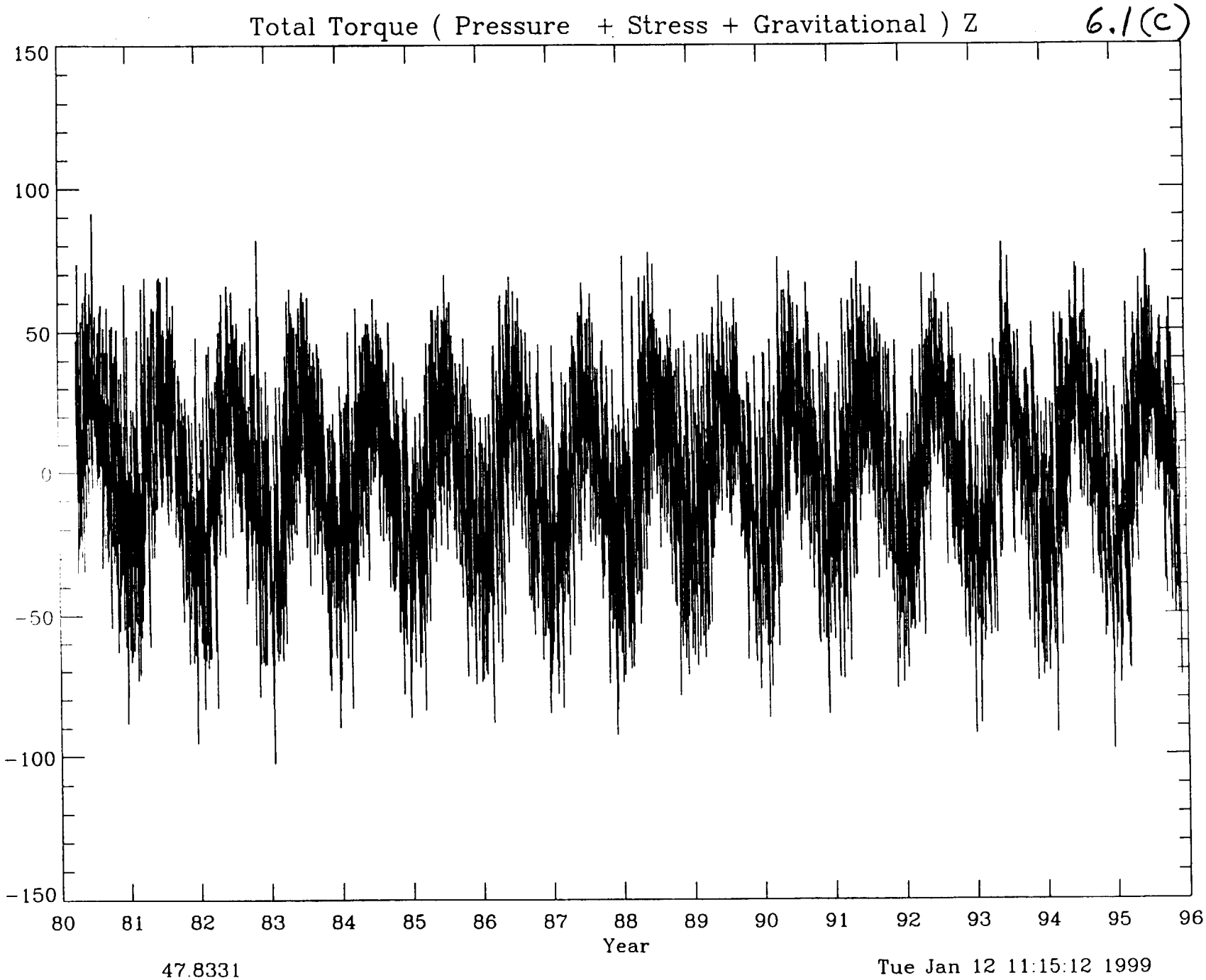
Total Torque (Pressure + Stress + Gravitational) Z
6.1(c)
150
100
50
0
-50
-100
-150
80
81
82
83
84
85
86
87
88
89
90
91
92
93
94
95
96
Year
47.8331
Tue Jan 12 11:15:12 1999

6.2(a)

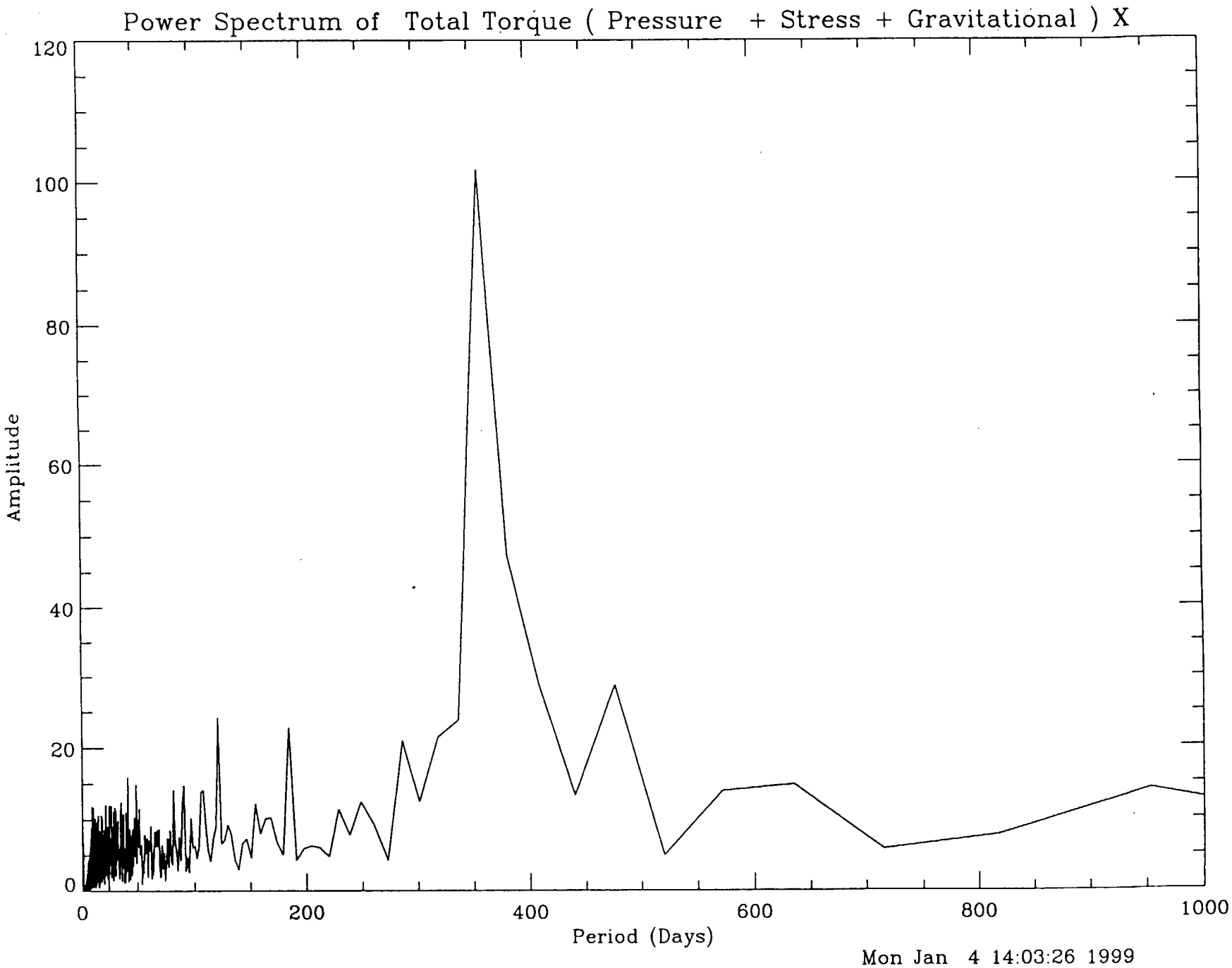
Power Spectrum of Total Torque (Pressure + Stress + Gravitational) X
Amplitude
120
100
80
60
40
20
0
0
200
400
600
800
1000
Period (Days)
Mon Jan 4 14:03:26 1999

6.2 (b)

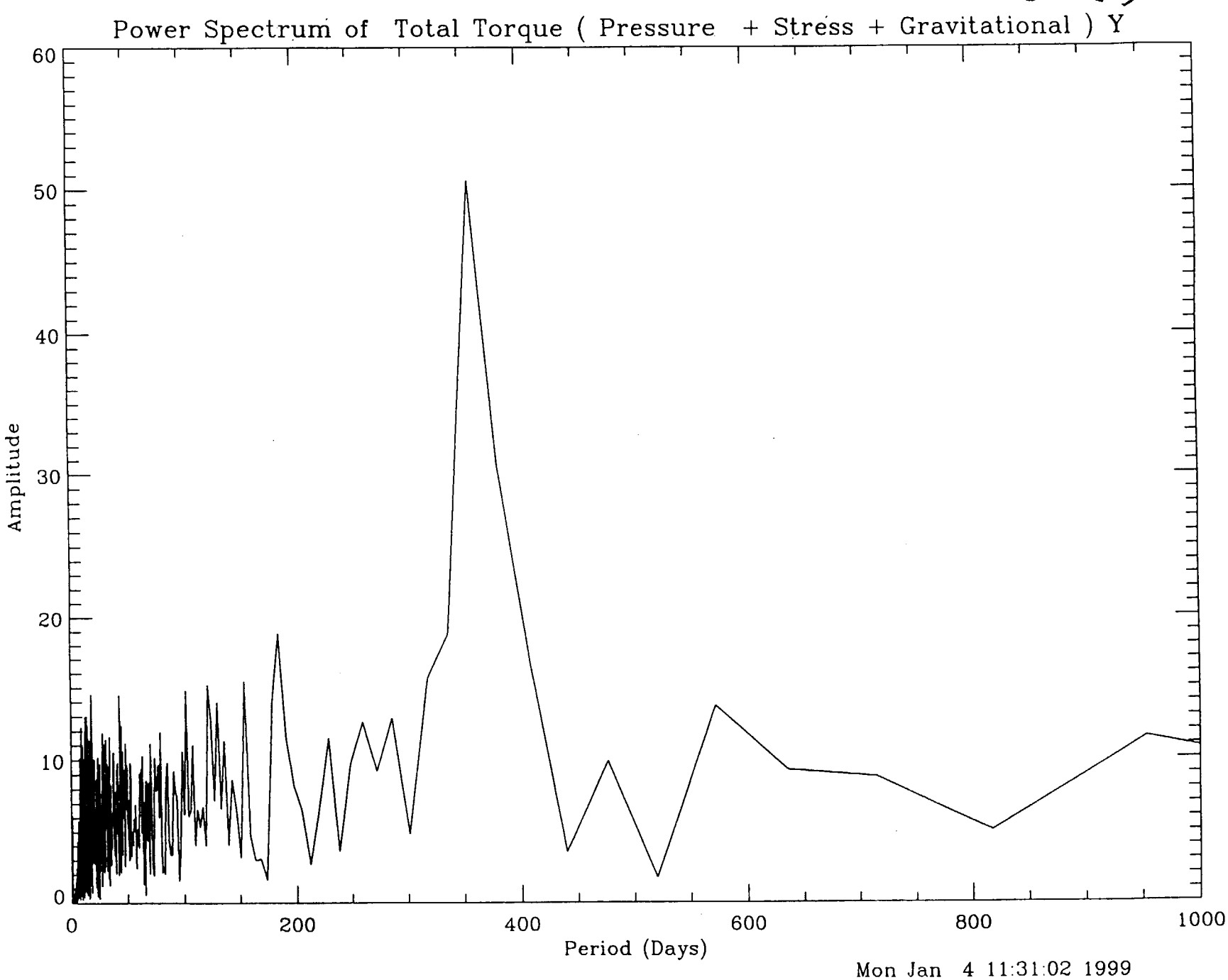
Power Spectrum of Total Torque (Pressure + Stress + Gravitational) Y
Amplitude
0
10
20
30
40
50
60
0
200
400
600
800
1000
Period (Days)
Mon Jan 4 11:31:02 1999

6.2(c)

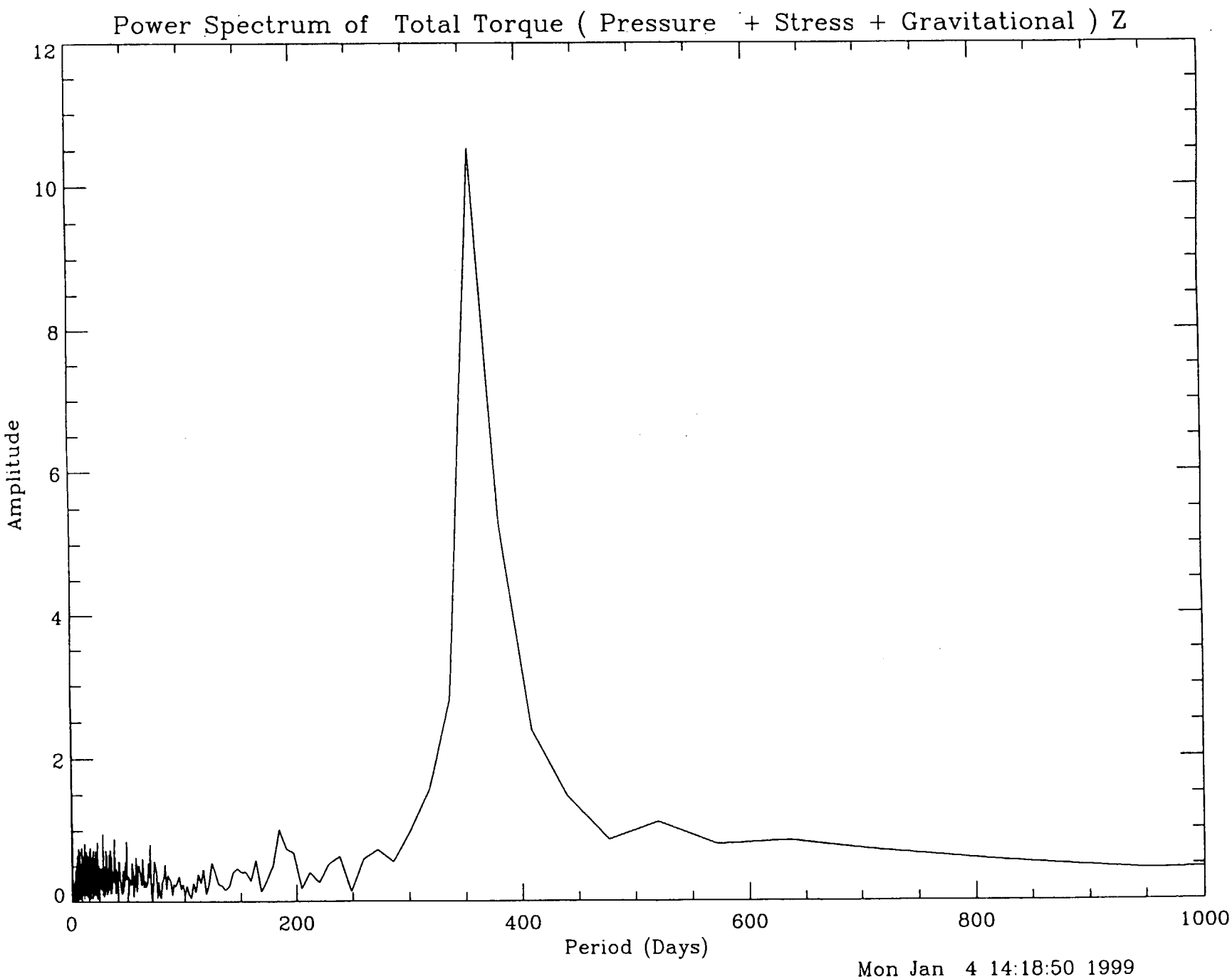
Power Spectrum of Total Torque (Pressure + Stress + Gravitational) Z
Amplitude
0
2
4
6
8
10
12
0
200
400
600
800
1000
Period (Days)
Mon Jan 4 14:18:50 1999

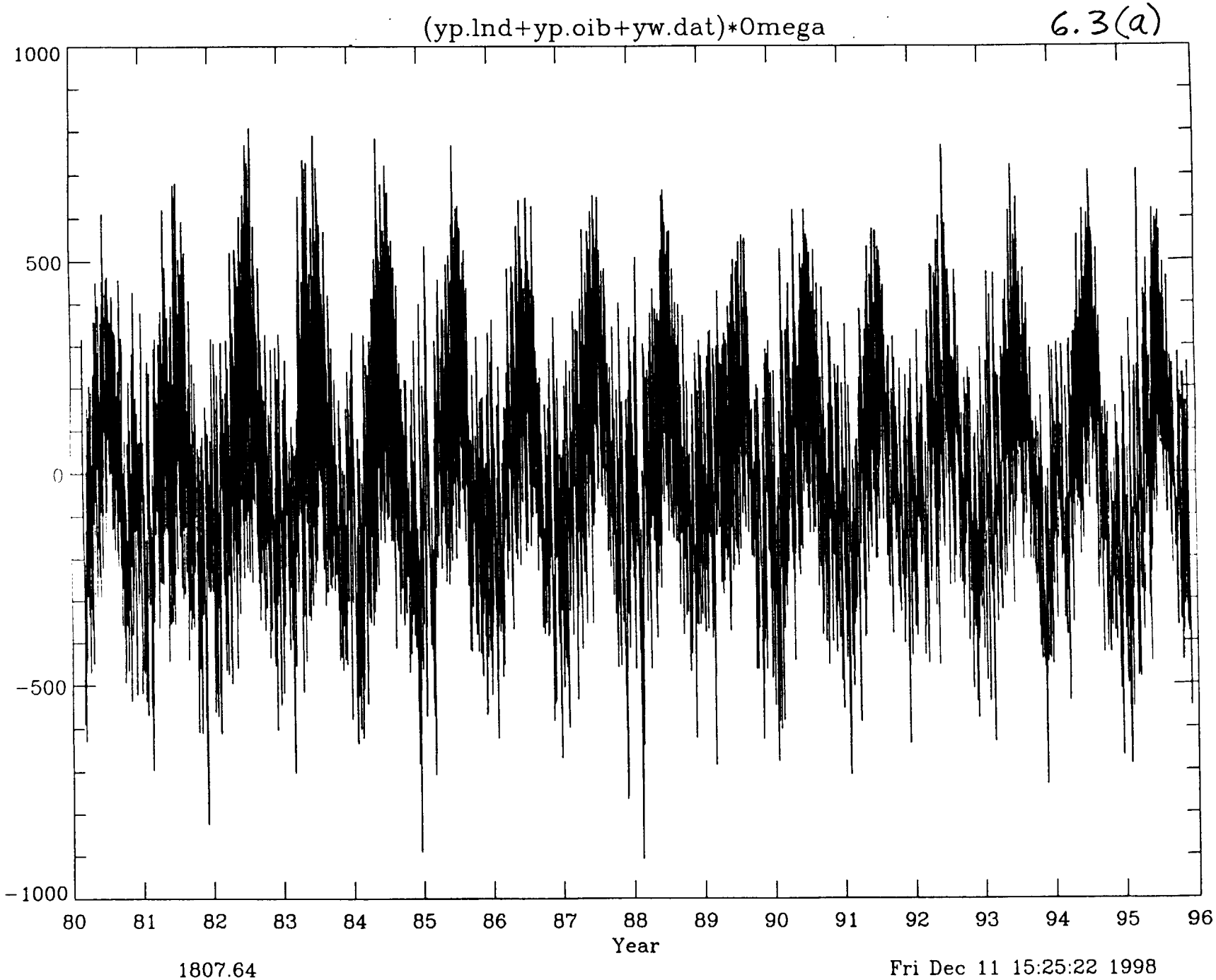
(yp.lnd+yp.oib+yw.dat)*Omega
6.3(a)
1000
500
0
-500
-1000
80
81
82
83
84
85
86
87
88
89
90
91
92
93
94
95
96
Year
1807.64
Fri Dec 11 15:25:22 1998

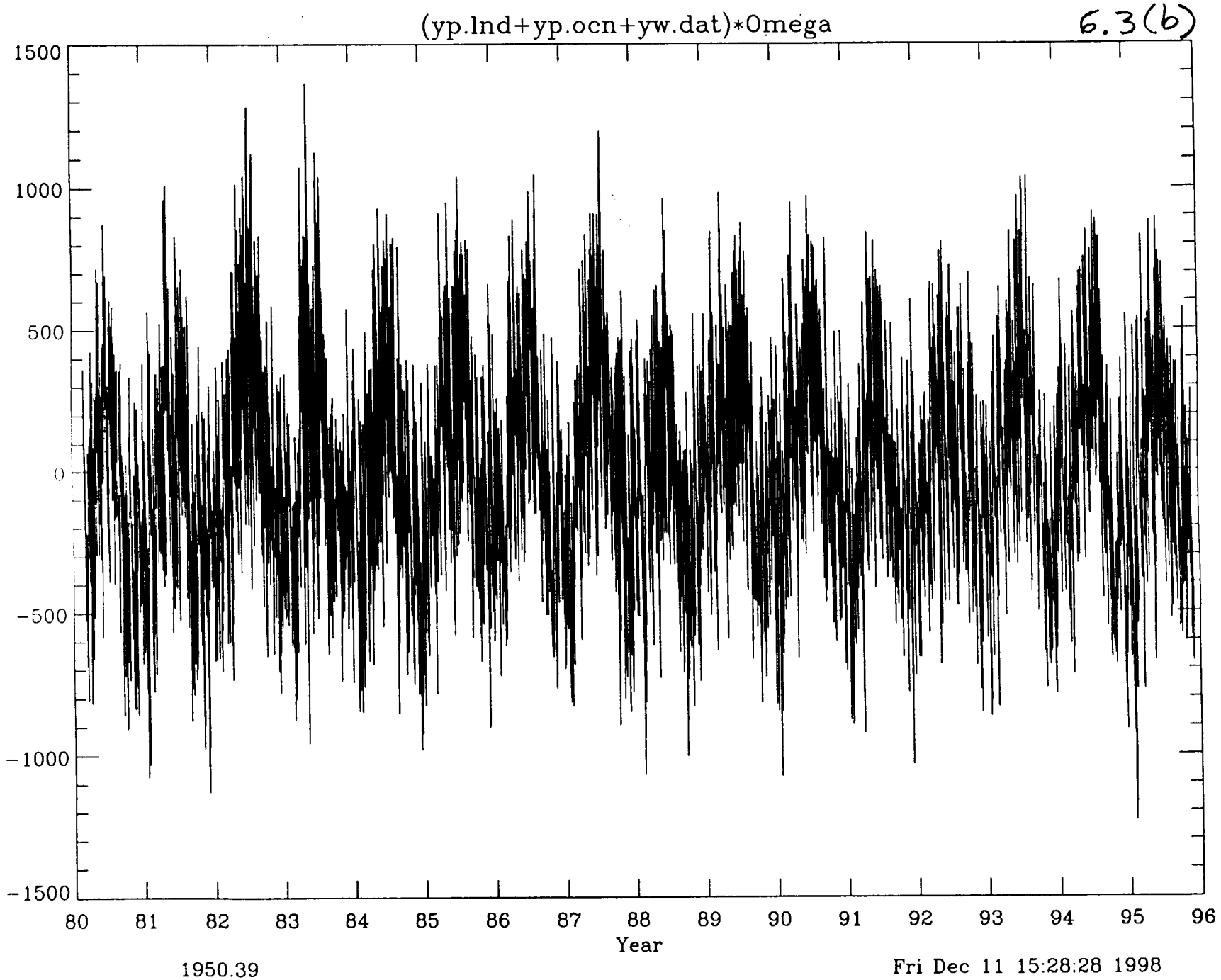
(yp.lnd+yp.ocn+yw.dat)*Omega
6.3(b)
1500
1000
500
0
-500
-1000
-1500
80
81
82
83
84
85
86
87
88
89
90
91
92
93
94
95
96
Year
1950.39
Fri Dec 11 15:28:28 1998